

**The G4Foam Experiment:
Global Climate Impacts of Regional Ocean Albedo Modification**

Corey J. Gabriel^{1*}, Alan Robock¹, Lili Xia¹, Brian Zambri¹, and Ben Kravitz²

¹Department of Environmental Sciences, Rutgers University, New Brunswick, NJ, USA

²Atmospheric Sciences and Global Change Division, Pacific Northwest National Laboratory,
Richland, Washington, USA

1
2

Submitted to *Atmospheric Chemistry and Physics*
Special Issue: The Geoengineering Model Intercomparison Project

September, 2016

Revised December, 2016

*To whom correspondence should be addressed: Corey J. Gabriel, Department of Environmental Sciences, Rutgers University, 14 College Farm Road, New Brunswick, NJ 08901-8551. E-mail: corey@envsci.rutgers.edu.

3

4 **Abstract.** Reducing insolation has been proposed as a geoengineering response to global
5 warming. Here we present the results of climate model simulations of a unique Geoengineering
6 Model Intercomparison Project Testbed experiment to investigate the benefits and risks of a
7 scheme that would brighten certain oceanic regions. The National Center for Atmospheric
8 Research CESM-CAM4-CHEM global climate model was modified to simulate a scheme in
9 which the albedo of the ocean surface is increased over the subtropical ocean gyres in the
10 Southern Hemisphere. In theory, this could be accomplished using a stable, nondispersive foam,
11 comprised of tiny, highly reflective microbubbles. Such a foam has been developed under
12 idealized conditions, although deployment at a large scale is presently infeasible. We conducted
13 three ensemble members of a simulation (G4Foam) from 2020 through 2069 in which the albedo
14 of the ocean surface is set to 0.15 (an increase of 150%) over the three subtropical ocean gyres in
15 the Southern Hemisphere, against a background of the RCP6.0 (representative concentration
16 pathway resulting in $+6 \text{ W m}^{-2}$ radiative forcing by 2100) scenario. After 2069, geoengineering
17 is ceased, and the simulation is run for an additional 20 years. Global mean surface temperature
18 in G4Foam is 0.6 K lower than RCP6.0, with statistically significant cooling relative to RCP6.0
19 south of 30°N . There is an increase in rainfall over land, most pronouncedly in the tropics during
20 the June-July-August season, relative to both G4SSA (specified stratospheric aerosols) and
21 RCP6.0. Heavily populated and highly cultivated regions throughout the tropics, including the
22 Sahel, Southern Asia, the Maritime Continent, Central America and much of the Amazon,
23 experience a statistically significant increase in precipitation minus evaporation. The
24 temperature response to the relatively modest global average forcing of -1.5 W m^{-2} is amplified
25 through a series of positive cloud feedbacks, in which more shortwave radiation is reflected. The
26 precipitation response is primarily the result of the intensification of the southern Hadley cell, as
27 its mean position migrates northward and away from the Equator in response to the asymmetric
28 cooling.
29

30 **1 Introduction**

31 **1.1 Background**

32 The current rate of increase in global mean surface temperature is unprecedented in the
33 last 1,000 years (Marcott et al., 2013). The atmospheric concentration of CO₂ is higher now than
34 at any time in the last 650,000 years (Siegenthaler et al., 2005). It is extremely likely that the
35 warming since 1950 is primarily the result of anthropogenic emission of heat-trapping gases
36 rather than natural climate variability (IPCC, 2013). Motivated by insufficient progress in
37 setting and achieving mitigation targets, solar radiation management (SRM) has been proposed
38 as a method of reducing global mean temperature, thereby ameliorating many of the negative
39 effects of global warming (Crutzen, 2006). The most discussed SRM approach involves
40 injection of sulfur dioxide (SO₂) into the tropical stratosphere. Other suggested SRM
41 geoengineering methods include marine cloud brightening (Jones et al., 2009; Rasch et al., 2009;
42 Latham et al., 2010) and surface albedo modification (Irvine et al., 2010; Cvijanovic et al.,
43 2015). Each of these methods has the potential to cool Earth's surface, but each comes with
44 known potential side effects. For example, Robock (2008, 2014, 2016) enumerated and
45 described specific risks and benefits of stratospheric geoengineering.

46 Here we present a Geoengineering Model intercomparison Project (GeoMIP) testbed
47 experiment (Kravitz et al., 2011, 2016), consisting of the novel implementation of an ocean
48 surface albedo modification scheme in a climate model, which simulates the placement of a
49 reflective foam, consisting of microbubbles, on the ocean surface. RCP6.0 and G4SSA are run
50 with an ocean surface albedo with a very small diurnal cycle, and the daily average albedo is
51 very close to 0.06. In our experiment, the albedo of the ocean surface is raised from this daily
52 mean of 0.06 to a constant value of 0.15, with no daily cycle, over the subtropical ocean gyres in
53 the Southern Hemisphere, specifically 20°N-20°S, 90°W-170°W (South Pacific), 20°N-20°S,
54 30°W-0°E (South Atlantic) and 20°N-20°S, 55°E-105°E (South Indian) (Fig. 1). Everywhere
55 else, ocean surface albedo in G4Foam is calculated in the same way as in RCP6.0 and G4SSA.
56 It is possible that the absence of a small daily cycle in albedo would result in a slightly different
57 surface energy budget than would occur if the foamed regions exhibited variations in albedo.
58 However, the foamed regions' albedos would likely fluctuate as a function of many things,
59 including some movement of the foam itself, foam interaction with precipitation or aerosols,
60 wind speed, and sun angle. Further study of the properties of the foam, including in ocean water
61 with some turbulence, could provide information that would allow future modeling of the foam
62 to include albedo fluctuations. This is the G4Foam experiment, which simulates a particular
63 implementation of an idealized form of the technology described by Aziz et al. (2014), where
64 stable, reflective foam suitable for use as SRM in ocean regions with limited nutrients that
65 support little marine life is made in the laboratory.

66 The broad idea of microbubble deployment as a form of SRM is explored by Seitz
67 (2010). Here we only examine the potential benefits and risks of such a scheme, and do not
68 advocate deployment of any form of geoengineering regardless of its present feasibility. Robock
69 (2011) has cautioned against the potential implications of ocean albedo modification as presented
70 by Seitz (2010).

71 Stratospheric sulfate injection (SSI) is the most discussed form of geoengineering and,
72 given the current state of research, the most feasible (Dykema et al., 2014, Keith et al., 2014).
73 Implementation of the G4Foam regional ocean albedo modification scheme could be considered
74 with or without concurrent SSI. G4Foam could be used as a potential SSI concurrent scheme
75 aimed at correcting possible adverse impacts on the hydrological cycle brought about by ongoing
76 SSI. G4Foam is also a potential alternative to SSI with a far different latitudinal distribution of

77 benefits. The focus here is solely on the second scenario, as it allows for the elucidation of the
78 impacts of the G4Foam experiment forcing alone.

79 **1.2 Motivation and Research Question**

80 Is it possible to cool the planet while concurrently maintaining or increasing precipitation
81 in highly populated and heavily cultivated regions, particularly in regions dependent on monsoon
82 precipitation? We begin by determining whether a forcing can be applied in a global climate
83 model (GCM) that will result in the model responding with a northward and landward shift of
84 tropical precipitation needed to achieve our objective. To that end we conducted simulations
85 with The Community Earth System Model 1/Community Atmospheric Model 4 fully coupled to
86 tropospheric and stratospheric chemistry (CESM1 CAM4–Chem) model (Lamarque et al., 2012;
87 Tilmes et al., 2015, 2016). We ran the model with horizontal resolution of $0.9^\circ \times 1.25^\circ$ lat-lon
88 and 26 levels from the surface to about 40 km (3.5 mb), as was done for G4SSA (specified
89 stratospheric aerosol) by Xia et al. (2016).

90 The experiments consisted of three ensemble members of a simulation from 2020-2089 in
91 which the ocean surface albedo is raised as described above from an average of 0.06, which
92 includes a small diurnal cycle of albedo, to a daytime constant 0.15 on the SH subtropical ocean
93 gyres for 50 years, 2020-2069, and then returned to unforced values from 2070-2089 to assess
94 termination. Our hypothesis is that the tropical rain belts will move northward largely as a result
95 of increased moisture convergence over land regions, particularly during Northern Hemisphere
96 (NH) summer (June-July-August, JJA) in NH monsoon regions. Enhanced divergence over the
97 already strong subtropical highs, due to increased subsidence over the increased albedo ocean
98 regions in the subtropical Southern Hemisphere (SH), would help the cooler air from the forced
99 subtropical regions advect throughout the SH troposphere.

100 The asymmetric cooling would force changes in the Hadley Cell, enhancing cross-
101 equatorial flow, which would cool the surface in the NH tropics, especially during JJA, when
102 heat mortality and morbidity is highest. However, despite a reduction in the JJA mean
103 temperature in the tropics, extreme events are responsible for most heat-related mortality and
104 morbidity, and the reduction in the mean temperature does not necessarily mean that there will
105 be a reduction in the type of extreme heat events that cause human tragedy. While Kharin et al.
106 (2007) showed that, in general, temperature extremes track with the mean temperature, this is not
107 always the case. The changes in extreme events may, for example, be greater at high latitudes
108 and the variability of temperatures over land may increase in a warmer climate.

109 Specific to geoengineering, Aswathy et al. (2015) showed that different climate
110 engineering methods produce spatially heterogeneous changes in extreme precipitation and
111 temperature events. They showed that one SRM scheme may be more effective than another in
112 reducing different types of extreme events despite relatively similar global and regional mean
113 responses. In particular, a marine cloud brightening scheme that brightens ocean areas between
114 30°N and 30°S is shown to be less effective in reducing extreme precipitation and temperature
115 events over land than the G3 experiment is.

116 Finally, the resulting cooling of low latitude NH land areas would not dampen the
117 monsoon. The wet season monsoon circulation is initiated and maintained by the moist static
118 energy gradient, not the surface temperature gradient. A wetter, more cloudy land mass will
119 strengthen, not dampen the circulation relative to a warmer, drier continent (Hurley and Boos,
120 2014), especially with a cooler, lower specific humidity environment under the descending
121 branch of the meridional circulation.

122 The strength of this response will be very sensitive to any cloud feedbacks that result
123 from the surface albedo forcing. The basis of this comprehensive hypothesis is described in

124 detail, below, specifically in sections 1.3 and 1.4. The details of the experiment are discussed in
125 detail in section 2.

126 **1.3 Stratospheric geoengineering weakens the hydrological cycle**

127 With global warming, low-level specific humidity will increase by about $7\% K^{-1}$ within
128 the tropical planetary boundary layer. This response will be spatially homogeneous throughout
129 the tropics. However, the precipitation response will be different. Increased moisture
130 convergence in areas that already get a lot of precipitation will result in the “wet getting wetter,”
131 while increased moisture divergence in dry areas will result in the “dry getting drier” (Held and
132 Soden, 2006).

133 The “rich get richer, poor get poorer” paradigm does not hold up in an SRM world, where
134 the response is very different from that under global warming. Based on the results of an
135 observational study, Trenberth and Dai (2007) pointed out the possibility that drought,
136 particularly in the tropics, could result from geoengineering. Tilmes et al. (2013) analyzed the
137 hydrological cycle in most of the GeoMIP participating Coupled Model Intercomparison Project
138 5 (CMIP5) (Taylor et al., 2012) models by comparing abrupt $4xCO_2$, piControl, and G1. They
139 found a robust reduction in global monsoon rainfall, including in the Asian and West African
140 monsoon regions in G1 relative to both abrupt $4xCO_2$ and piControl. Haywood et al. (2013)
141 explored the impact of SSI in one hemisphere only and found a movement of the ITCZ away
142 from the hemisphere that was cooler as a result of the asymmetric SSI.

143 This consensus about the potential for less tropical rainfall under a regime of
144 stratospheric SRM motivates us to identify an alternative or SSI-adjunctive geoengineering
145 approach that could cool the planet, without reducing monsoon precipitation in highly cultivated
146 areas.

147 **1.4 Extratropical forcing impacts the position of the ITCZ**

148 Under global warming tropical rainbelts will move toward the hemisphere that warms
149 more (Chiang and Bitz, 2005, Frierson and Hwang, 2012). This ITCZ migration was first seen in
150 early atmosphere-ocean coupled models. Clouds were prescribed in those models, and when
151 clouds were changed in such a way to preferentially cool one hemisphere, the ITCZ responded to
152 changes by moving toward the warmer hemisphere. Increasing low cloud cover, and thereby
153 inducing cooling, in one hemisphere relative to the other caused the tropical rainbelts over the
154 Pacific Ocean to move toward the other hemisphere (Manabe and Stouffer, 1980). The impacts
155 of asymmetric heating of the hemispheres became highly relevant during the Sahel drought.
156 Much of the rainfall deficit during the devastating 20-30 year drought can be attributed to
157 cooling initiated by increased tropospheric sulfate emissions in the NH (Hwang et al., 2013).
158 The forced cooling over the NH was enhanced by a positive dynamical feedback in the North
159 Atlantic Ocean. (Broccoli et al. 2006; Kang et al. 2008) and the ITCZ and associated tropical
160 rainbelts migrated south. Since the Sahel is at the northern margin of the ITCZs annual
161 migration, or at the northern terminus of the West African monsoon, southward displacement of
162 the ITCZ led to a devastating drought (Folland, 1986).

163 Broccoli et al. (2006) diagnosed the energy balance mechanism that causes the ITCZ to
164 shift in response to asymmetric heating of the extratropics. Using models of varying complexity,
165 Broccoli et al. (2006) imposed an anomalous cooling of the NH, either via a last glacial
166 maximum simulation, or via hosing of the North Atlantic. The heating asymmetry causes the
167 extratropics in the NH to demand more heat and the extratropics in the SH to demand less heat.
168 Since cross equatorial heat transport is achieved principally via the Hadley Cell, the SH Hadley
169 Cell strengthens, particularly in austral summer, in response to the NH cooling, and net energy
170 flow in the upper branch intensifies, redistributing energy into the NH from the relatively warm
171 SH.

172 Net flow of energy in the Hadley cell can be described in terms of the flow of moist static
173 energy, which flows in the direction of the upper troposphere branch of the Hadley Cell. This is
174 because moist static energy is higher at higher altitudes in the troposphere due to the increased
175 contribution of the geopotential energy term overwhelming the moisture and internal energy
176 terms in the moist static energy equation for the high altitude air. Net transport of energy,
177 occurring in the upper branch of the Hadley cell from the SH to the NH, leads to increased
178 moisture advection to the SH in the lower branch of the Hadley Cell. This redistribution of
179 energy causes the ascending branch of the Hadley cell to migrate to the warmer SH where
180 moisture convergence is increased and convective quasi-equilibrium is achieved under the
181 relatively narrow poleward shifted ascending branch of the stronger SH winter Hadley Cell.
182 This mechanism leads to the southward-displaced tropical rain belts (Broccoli et al., 2006).

183 This result is consistent with Lindzen and Hou (1988), who used a relatively simple
184 model to show that even a small movement of maximum heating poleward into one hemisphere
185 causes great asymmetry in the Hadley Cell, with the winter cell intensifying tremendously and
186 the summer cell becoming rather modest. More recent work continues to elucidate the
187 mechanism of extratropical forcing of the ITCZ (Kang et al. 2008). The ocean also plays a vital
188 role in pushing the ITCZ into the warmer hemisphere (Xie and Philander, 1994).

189 GCM results confirm this mechanism and connect the changes due to northward
190 displacement of the ITCZ with the onset of active periods in the Asian summer monsoon (Chao
191 and Chen 2001). It is evident that a geoengineering technique that could preferentially cool the
192 SH could shift the tropical rain bands northward. However, in a GCM there are clouds. How
193 would clouds respond in the hemisphere cooled by geoengineering? Would clouds change in the
194 area being directly cooled? Would a cooling of the subtropics either directly, or indirectly via
195 eddy flux from the artificially cool high latitudes, cause an increase in subtropical subsidence?
196 Would this increase in the sinking of air above the intensified subtropical highs cause water
197 vapor to be trapped in the lower troposphere, forming low clouds and suppressing water vapor
198 mixing into the free troposphere, where the water vapor may instead be used up in formation of
199 high clouds, which tend to reduce outgoing longwave radiation? Informed by these established
200 diagnostic mechanisms associated with the impacts of asymmetric heating of the hemispheres,
201 we seek to concurrently cool the entire SH and the NH tropics, modestly cool the NH
202 extratropics and, most importantly, induce an anomalous overturning circulation and redistribute
203 rainfall from ocean to land and from south to north across the tropics.

204 **2. Methods**

205 **2.1 Design of experiment and model configuration**

206 Figure 1 shows the regions selected for albedo enhancement. These regions were chosen
207 because of their low cloud fraction, low wind speeds, weak currents, and lack of biological
208 productivity.

209 We used the Community Land Model (CLM) version 4.0 with prescribed satellite
210 phenology (CLM4SP) instead of the version of CLM with a carbon–nitrogen cycle, coupled with
211 CAM4–chem. Vegetation photosynthesis is calculated under the assumption of prescribed
212 phenology and no explicit nutrient limitations (Bonan et al., 2011, Xia et al., 2016). Dynamic
213 vegetation is not turned on in this study. The ocean model does not include any biogeochemical
214 responses.

215 The fundamental question we wish to answer concerns representation of the physical
216 processes that lead to realistic simulation tropical precipitation. The Asian monsoon is of great
217 importance in that investigation. Fortunately, monsoon processes and regimes are depicted well
218 in our atmospheric component, CAM4 (Meehl et al., 2012). Some important features of CAM4
219 that illustrate its very good monsoon representation include the amount and location of

220 precipitation over the southern Tibetan Plateau and over the Western Ghats (a mountain range
221 near the west coast of south India). This is improved when compared to earlier versions of the
222 model. The rain shadow leeward of this range is often not resolved by GCMs, however CAM4
223 shows some evidence of this rain shadow. These changes related to orography and horizontal
224 resolution are important and likely generalize to similar land surface features outside of India,
225 where model biases have not been as carefully studied as they have been in heavily populated
226 southern India. This improvement can be attributed to the CCSM4 finite-volume dynamical
227 core, which replaces the spectral version of the CCSM3 and the interconnected higher horizontal
228 resolution (Neale et al., 2013). Additionally, large-scale features are improved. For example,
229 the representation of the ITCZ during NH winter southward migration over the maritime
230 continent is improved (Meehl et al., 2011).

231 There is an important process associated with monsoon precipitation, however, that may
232 be imperfectly simulated across many CMIP5 GCMs. Zonal mean absorbed shortwave radiation
233 is too high over the southern ocean (Kay et al., 2016). This cloud problem leads to a warmer
234 Southern Ocean, which leads to anomalous SH atmospheric eddy flux to the subtropics from the
235 extratropics, potentially damping the cooling response of our negative surface radiative forcing
236 in the subtropical oceans. The effect of a transfer of heat from the SH extratropics into the
237 Hadley Cell already causes a relatively weak negative bias in the amount of interhemispheric
238 heat transport from the south to north. Therefore, the manifestation of this bias in G4Foam
239 would be to partially offset our imposed cooling, lessening the need for interhemispheric energy
240 transport to the SH and suppressing the surface return flow of moisture advection into the NH.
241 Lower than observed interhemispheric energy transport would be associated with a weaker Asian
242 monsoon. However, this feature is equally present in our G4Foam experiment and the
243 comparison experiments G4SSA and RCP6.0, so is unlikely to appreciably affect the differences.

244 We compare G4Foam to two experiments. First is a specific sulfate injection scenario,
245 G4 Specified Stratospheric Aerosol (G4SSA; Xia et al., 2016). They used a prescribed
246 stratospheric aerosol distribution roughly analogous to annual tropical emission into the
247 stratosphere (at 60 mb) of 8 Tg SO₂ yr⁻¹ from 2020 to 2070. This produces a radiative forcing of
248 about -2.5 W m⁻². The G4SSA forcing ramps down from 2069-2071 and then continues without
249 additional forcing from 2072-2089. In G4SSA tropospheric aerosols are not affected by the
250 prescribed stratospheric aerosols. Therefore we cannot evaluate how stratospheric aerosols
251 would actually fall out and impact the chemistry, dynamics and thermodynamics of the
252 troposphere from this experiment. Neely et al. (2015) offers more detail on the prescription of
253 stratospheric aerosols in CAM4-Chem. The second simulation for comparison, which serves as
254 the reference simulation, for both G4Foam and G4SSA is the Representative Concentration
255 Pathway 6.0 (RCP6.0) (Meinshausen et al., 2011) from 2004 to 2089. We have run three
256 ensemble members each for G4Foam, G4SSA, and RCP6.0.

257 **2.2 Ocean albedo enhancement approach**

258 A plausible technology now exists to make quantities of long lasting foam, or engineered
259 microbubbles to enhance ocean albedo. . Ocean albedo modification gained attention when
260 Seitz (2010) suggested that since air-water and air-sea interfaces are similarly refractive,
261 dispersing microbubbles onto the surface of the ocean would reflect sunlight in much the same
262 way as cloud droplets do. While engineering refractive or stable foams is commonly done and
263 applied in both food science and firefighting, engineering a stable and refractive foam
264 appropriate for a geoengineering scheme appeared fanciful until Aziz et al. (2014) produced a
265 long lasting refractive foam made with biodegradable and non-toxic additives. Aziz et al.
266 identified foam lifetime of three months or more per microbubble as lasting long enough that the
267 input of energy to create the microbubbles would not be prohibitive. After experimenting with

268 protein-only solutions, Aziz et al. (2014) added high methyl ester pectin to type A gelatin and
269 created a foam in salt water, which was still intact and stable at the cessation of the experiment
270 after 3 months. The reflectance of the foam was about 50%, which is comparable to that of
271 whitecaps. The creation of these stable microbubbles makes enhancing ocean albedo in this
272 manner “feasible” (Aziz et al. 2014). However, there are a number of other potential risks
273 associated with microbubble deployment, even if the feasibility issues are set aside. Robock
274 (2011) pointed out that vertical mixing in the ocean, changes in ocean circulation, impacts on
275 photosynthesis, and risks to the biosphere could all impair the efficacy of this geoengineering
276 approach. Robock (2011) also pointed out that a cooler ocean would serve as a more effective
277 CO₂ sink, helping to offset the CO₂ increase that comes about as a feedback of warming. Other
278 potentially attractive attributes of this technique include the possibility that it could be deployed
279 exclusively in the 20% of the world’s oceans that are not biologically active (Aziz et al. 2014)
280 and therefore have little impact on the biosphere, and that there would be no risk to ozone in the
281 stratosphere.

282 **3 Results**

283 The following results compare the G4Foam climate with the climates in G4SSA and
284 RCP6.0 averaged over the period 2030-2069. While G4Foam and G4SSA forcing commences in
285 2020, the first ten years of both experiments are a period of transition. For that reason 2020-
286 2029 is discarded from our comparisons. We analyze mainly annual average and JJA results,
287 since JJA is meteorological summer in the NH and using JJA facilitates comparison with
288 G4SSA, which reports results in terms of JJA (Xia et al., 2016).

289 **3.1 Temperature and cloud response**

290 The primary purpose of G4Foam is to assess the possibility of reducing global mean
291 surface temperature without reducing monsoon precipitation. The G4Foam simulations reduce
292 global mean surface temperature relative to RCP6.0 by 0.60 K and global mean land surface
293 temperature by 0.51 K relative to RCP6.0. In JJA, G4Foam is 0.70 K cooler than RCP6.0 over
294 land in the tropics, 20°S-20°N, during JJA (Table 1).

295 These temperature changes in G4Foam, relative to RCP6.0, result from an all-sky top-of-
296 atmosphere forcing of -1.5 W m⁻² (global, year-round), and -1.9 W m⁻² in the tropics during JJA
297 only (Figure 2). This JJA cooling in the tropics is of particular importance due to the dense
298 population and heavy agricultural demand in the tropics, particularly north of the equator.

299 G4Foam does not achieve the same amount of cooling as G4SSA, which would reduce
300 global mean surface temperature by 0.92 K. All-sky top-of-atmosphere shortwave flux in G4SSA
301 is reduced by 2.7 W m⁻² as compared to RCP6.0. In terms of global mean clear-sky top-of-
302 atmosphere shortwave flux, relative to RCP6.0, G4Foam applies only 38% of the forcing that is
303 applied in G4SSA (Figure 3). The G4Foam forcing is more efficient in reducing temperature
304 than G4SSA largely because there is an additional 1.1 W m⁻² of net cloud forcing in G4Foam
305 relative to G4SSA (Figure 2b).

306 Figure 4 shows a comparison of the spatial distribution of surface temperature changes
307 between G4Foam and G4SSA and between G4Foam and RCP6.0 between 2030-2069. Over the
308 SH ocean gyres that were brightened (Fig. 1), we see a very robust cooling, reaching 2 K at the
309 center of the South Pacific foamed region. However, the cooling mixes rather well throughout
310 the SH. Cross equatorial flow and changes in the Hadley Cell transmit this cooling into the NH
311 tropics through the mechanisms described in section 1.4, above. Some of this cooling in the NH
312 tropics is then transmitted to the NH extratropics.

313 G4Foam is significantly cooler ($p < 0.05$) than RCP6.0 in almost all locations south of
314 30°N, in mid latitude NH continental regions windward of the Atlantic and Pacific, and at very
315 high latitudes. Figure 4d shows that G4Foam is less effective in cooling extratropical NH land

316 regions during JJA. This is reasonable, since continental heating in the NH JJA season is more
317 dominated by local heating than the other seasons, in which meridional energy transport plays a
318 larger role. Figures 4a and 4c show that G4SSA is more effective over NH continents than
319 G4Foam. A key weakness of G4Foam, if implemented alone, would be its failure to adequately
320 reduce human suffering induced by heat stress in NH mid-latitudes during the summer as a result
321 of ongoing global warming.

322 Since the G4Foam forcing alone, with the amplitude of the current experiments, would be
323 insufficient to achieve any of the objectives of the G4Foam experiment, positive feedbacks that
324 enhance cooling and circulation responses must be triggered by the G4Foam forcing to enhance a
325 resulting cooler, wetter climate. Figure 5 shows change in low cloud fraction both year-round
326 and in the JJA season. The largest change is in the northern half of the regions where foam is
327 applied, and the area to the north of those foamed regions. The changes in low clouds in these
328 regions are both large and statistically significant.

329 The low cloud fraction increase in the three areas to the north and northeast of the
330 G4Foam-forced subtropical surface regions is likely due to a stronger than normal trade wind
331 inversion (TWI). The inversion develops when warm air is trapped above the atmospheric
332 mixed layer due to large-scale subsidence and surface mixing of cooler air above these relatively
333 low SST regions. The increase in low cloud fraction does not occur over the entire downwind
334 area because SSTs increase from east to west, causing a change in the lower troposphere from
335 east to west. Moving west, the stratocumulus layer, which is trapped under the inversion base,
336 decouples from the mixed layer in the lower troposphere. The surface warming triggers more
337 turbulence within the planetary boundary layer, which allows for enhanced cumulus mixing in
338 the cloud layer, which entrains dry air, and the marine stratocumulus layer evaporates.

339 The subtropical high-pressure systems are stronger in G4Foam, due to the stronger than
340 normal Hadley Cell, which enhances subsidence throughout the subtropics. Typically, a
341 subsidence inversion is strongest over the center of the subtropical anticyclones, over cold
342 currents (particularly the Peru Current), and over cooler than normal waters, which are subjected
343 to enhanced upwelling in large part by trade winds on the periphery of the subtropical highs
344 (DeSzoeke et al., 2016). The TWI becomes weaker and its base increases in height with distance
345 towards the west and towards the equator as SSTs increase. This pattern is particularly evident
346 in the Pacific, due to the larger geographical extent of the forced area.

347 Specifically, under G4Foam conditions, the increased low cloud fraction areas are the
348 result of the combination of enhanced large-scale subsidence (stronger Hadley cell) and a cooler
349 than normal ocean surface. The cooler than normal surface waters are due to general cooling
350 throughout the SH, as well as an increase in wind-driven upwelling over these areas of increased
351 low cloud fraction, which are already prone to upwelling, large fraction of low clouds and high
352 relative humidity.

353 In these areas north of the foamed areas, the subsidence inversion is not quite as strong as
354 it is right under the subtropical high. However, SSTs are artificially low, due to general cooling
355 of the hemisphere and enhanced upwelling, driven by anomalously strong winds, and mixing of
356 this anomalously cool surface air within the planetary boundary layer keeps the lowest levels of
357 the atmosphere cool, keeping the marine air inversion base above the lifting condensation level,
358 allowing stratocumulus clouds to form at low altitude, below the base of the inversion.
359 Additionally, since SST is lower than air temperature in the areas of enhanced low clouds, the
360 surface inversion is further maintained as a result of sensible heat flux from the atmosphere to
361 the ocean. Ultimately, the strong inversion often results in more marine layer cloud formation
362 and longer times for the clouds to dissipate. This response is consistent through the 2030-2069
363 period. This enhanced low-cloud fraction response is similar to the seasonal cycle of marine low

364 clouds around the periphery of the subtropical highs (Wood and Bretherton, 2004; Chiang and
365 Bitz, 2005; Wood and Bretherton, 2006; George and Wood, 2010; Mechoso et al., 2014).

366 The relationship between the strength of the subtropical high, inversion strength and
367 marine cloud prevalence can be elucidated by analogy to the behavior of the very well-observed
368 marine low clouds off of the California coast. The strength of the inversion, and the prevalence
369 of marine low clouds are modulated by the annual cycle with annual maximum low cloud extent
370 in the summer, when the subtropical high is at its strongest. The increased low cloud fraction
371 response is not seen above the actual G4Foam forced regions despite the cooler SST. The
372 subsidence is so strong in these areas that the base of the inversion falls below the lifting
373 condensation level, and few clouds form (Fig. 5).

374 Another striking G4Foam feature is the large and statistically significant increase in low
375 clouds over land across central Africa, the Middle East and Southeast Asia. These low clouds
376 are coincident with the large cooling in Africa and the Middle East, particularly during the JJA
377 season relative to both G4SSA and RCP6.0 (Figs. 5c, 5d). These are very hot areas and heat
378 related mortality and morbidity are of great concern. A similar increase in low clouds is evident
379 in the tropical eastern Pacific. This is coincident with the mean northward displacement of the
380 ITCZ in G4Foam with respect to G4SSA and RCP6.0, not with any changes in the El Niño-
381 Southern Oscillation (ENSO).

382 In G4Foam, clouds are the key to changing the radiation budget in the tropics. In
383 G4Foam there is a change in shortwave cloud forcing of -2.32 W m^{-2} annually and -2.59 W m^{-2}
384 during JJA, relative to G4SSA. Only very small increases in longwave cloud forcing of 0.42 W m^{-2}
385 annually, and 0.07 W m^{-2} in JJA counter this negative forcing. The overall change in cloud
386 radiative forcing in the tropics is -1.90 W m^{-2} annually and -2.52 W m^{-2} during JJA. Relative to
387 RCP6.0, in G4Foam there is a change in shortwave cloud forcing of -0.68 W m^{-2} annually
388 and -0.89 W m^{-2} during JJA, relative to RCP6.0. Small increases in longwave cloud forcing of
389 0.40 W m^{-2} annually, and 0.28 W m^{-2} in JJA counter part of this negative forcing. The overall
390 change in cloud radiative forcing in G4Foam in the tropics is -0.49 W m^{-2} annually and -0.61 W m^{-2}
391 during JJA when compared to RCP6.0

392 Total cloud fraction is shown in Fig. 6. Figs. 6c and 6d are particularly striking in
393 showing the increase in clouds over Africa and Southeast Asia during the JJA wet monsoon
394 season in those regions. Under G4Foam, these regions generally experience cloudier and cooler
395 summers relative to RCP6.0 and are cloudier and only very slightly warmer on average
396 compared to G4SSA. Some parts of the Sahel and the Middle East are actually slightly cooler in
397 G4Foam than RCP6.0. These changes in temperature and cloudiness play a key role in the
398 changes in the hydrological cycle under G4Foam, which we discuss next.

399 **3.2 Hydrological Cycle Response**

400 Relative to G4SSA, precipitation in G4Foam over land in the tropics increases by 3.2%
401 on an annual mean basis and by 3.9% during JJA (Table 1). Tropical precipitation in G4Foam
402 over land in the tropics increases by 1.4% on an annual mean basis and by 2.02% during JJA,
403 when compared to RCP6.0. Each of these changes is statistically significant ($p < 0.05$).
404 Regarding the temperature change relative to G4SSA, G4Foam is only about 0.3 K warmer in
405 the tropics. Precipitation is expected to increase by between $1.5\% \text{ K}^{-1}$ and $3.0\% \text{ K}^{-1}$ as global
406 mean temperature increases (Emori and Brown, 2005). The temperature difference between
407 G4Foam and G4SSA can explain only a fraction of the precipitation increase. The statistically
408 significant increase in land-only precipitation in the tropics in G4Foam relative to RCP6.0 occurs
409 in a climate in which RCP6.0 is between 0.6 K and 0.7 K warmer than G4Foam, depending on
410 the season. Over the tropical oceans, in G4Foam, precipitation is reduced by 0.4% on an annual

411 mean basis and reduced by 0.3% during JJA relative to G4SSA. There is a decrease of 2.6% on
412 an annual mean basis and a decrease of 2.5% during JJA relative to RCP6.0.

413 Globally, over land, the precipitation response is similar to that in the tropics during JJA,
414 but the magnitude of precipitation change is a bit less. Precipitation is statistically significantly
415 increased over land in G4Foam relative to RCP6.0 by about 0.5%, despite G4Foam being cooler
416 than RCP6.0. Precipitation is statistically significantly increased in G4Foam relative to G4SSA
417 over land by 3.5%, despite G4Foam only being 0.3K warmer than G4SSA.

418 The overall global precipitation difference between G4Foam and G4SSA or RCP6.0
419 when land and ocean are combined and all seasons and all latitudes are included is relatively
420 small, and close to the 1.5% K⁻¹ to 3% K⁻¹ range of precipitation increase with temperature
421 identified by Emori and Brown (2005). Globally, G4Foam is warmer than G4SSA by 0.3 K and
422 there is 0.61% (2.1% K⁻¹) more precipitation. G4Foam is cooler than RCP6.0 by 0.6 K and drier
423 by 1.9% (3.1% K⁻¹).

424 The spatial pattern of precipitation changes is shown in Fig. 7. Precipitation is greatly
425 reduced over the ocean, particularly in the SH, relative to both G4SSA and RCP6.0. Changes in
426 precipitation poleward of 40° latitude in either hemisphere are largely due to the temperature
427 dependence of precipitation. The changes in the SH subtropics are dominated by the shortwave
428 forcing applied over the ocean gyres, which reduces both evaporation and precipitation in those
429 areas.

430 The changes in precipitation in the tropics are driven by a northward shift in the ITCZ.
431 Large precipitation anomalies occur in a narrow band north of the equator and smaller positive
432 anomalies occur in broader regions, primarily over NH monsoon regions. Importantly, we see a
433 statistically significant increase in monsoon precipitation over the Sahel, the Middle East, the
434 Indian subcontinent as well as southwest Asia and the maritime continent on an annual mean
435 basis in G4Foam relative to G4SSA (Figure 7a). Relative to RCP6.0, these changes are not
436 statistically significant over the Indian subcontinent or southwest Asia, but there are only very
437 isolated and small areas in these regions in which there is any precipitation reduction, either on
438 the annual mean or during JJA. Therefore, over much of heavily populated southern Asia, east
439 of the Arabian Sea, G4Foam will be cooler than RCP6.0 without any notable mean precipitation
440 differences. Most of these areas are expected to receive more rainfall as the planet warms. If
441 this excess rainfall is not desirable in areas that are already wet, these results suggest that
442 weakening the hydrological cycle would require that G4Foam would have to be combined with
443 an additional geoengineering technique, such as stratospheric SRM.

444 Relative to both G4SSA and RCP6.0, there is a great deal more precipitation all year and
445 particularly during JJA over central America, the northern Amazon, much of Africa, parts of the
446 Arabian peninsula and the maritime continent. This response is more robust than the response
447 over Southeast Asia due to the more direct dependence of rainfall in these regions on ITCZ
448 position than in Southeast Asia, where the monsoon is also driven by numerous local and remote
449 factors, including ENSO and the Indian Ocean Dipole.

450 Although these G4Foam simulations are enhance rainfall over many heavily populated
451 and highly cultivated regions, particularly in the tropics, there are regions that would receive less
452 precipitation and experience a decrease in P-E under this regime. Precipitation patterns for
453 islands in the South Pacific are largely governed by the position and strength of the South Pacific
454 Convergence Zone (SPCZ), which changes substantially under G4Foam due in part to the
455 cooling and to the movement of gradients of temperature and pressure. Precipitation deficits
456 over Madagascar and some regions in Africa and South America exceed 10%.

457 While the changes in precipitation are important and useful in describing the climate
458 response in G4Foam, the change in precipitation minus evaporation between G4Foam and

459 G4SSA or RCP6.0 is more relevant to total available moisture. Figure 8 shows precipitation
460 minus evaporation. Specifically Fig. 8a shows that precipitation minus evaporation in G4Foam
461 is increased, and this increase is significant relative to G4SSA, across the Sahel, all of South
462 Asia, the Maritime Continent, Central America and the northern Amazon. These are all heavily
463 populated regions that are heavily cultivated. Figure 8b shows a similar pattern, albeit with the
464 regions with significantly higher P-E is slightly suppressed in coverage, when G4Foam is
465 compared to the warmer RCP6.0 rather than G4SSA. Figures 8c and 8d show changes in P-E
466 during JJA, the NH wet monsoon season, when water is likely needed the most. Due to
467 variability in the monsoon, there is more heterogeneity in the JJA response than the annual
468 response, particularly across Southeast Asia. The P-E gain, driven by a combination of increased
469 precipitation, lower temperature and increased cloudiness in these heavily cultivated regions,
470 could be an important benefit of G4Foam. However, G4Foam increased precipitation to levels
471 that exceed that simulated in RCP6.0.

472 Figure 9 shows the differences of annual cycles from 2030-2069 for zonal mean
473 precipitation, zonal mean precipitation minus evaporation, and zonal mean precipitable water
474 between G4Foam and G4SSA and between G4Foam and RCP6.0. They illustrate the northward
475 displacement of the ITCZ, with positive precipitation anomalies progressing poleward as the
476 boreal summer monsoon progresses. Figure 9f shows the difference in the zonal mean annual
477 cycle for column integrated precipitable water between G4Foam and RCP6.0. The striking
478 feature here is that zonal mean precipitation is higher at key latitudes in the tropics, despite zonal
479 mean column integrated precipitable water being much lower at the same latitude.

480 In Fig. 10, we quantify the impacts on agriculture by looking at the photosynthesis rate
481 anomalies between G4Foam and RCP6.0. There are small, but statistically significant increases,
482 in photosynthesis rate in G4Foam relative to RCP6.0 in much of Southeast Asia. The most
483 dramatic changes occur in Central America and parts of the northern Amazon, where the high
484 CO₂, relatively cool and very wet conditions promote agriculture.

485 **4 Discussion**

486 This paper is an analysis of a geoengineering climate model experiment. Although for
487 this experiment, global warming is reduced without seriously affecting precipitation, as was
488 found in previous stratospheric aerosol implementations, this does not argue for the
489 implementation of climate engineering. Any such decisions will need to balance all the risks and
490 benefits of such implementation, and compare them to those from other possible responses to
491 global warming.

492 **4.1 Summary**

493 G4Foam would reduce global mean surface temperature relative to RCP6.0 by 0.6 K for
494 the 40-year period starting 10 years after the implementation of geoengineering. Clear sky top of
495 atmosphere net shortwave flux is reduced by 1.5 W m⁻² in G4Foam relative to RCP6.0. This is
496 achieved primarily by the shortwave forcing over the subtropical SH ocean gyres. Before
497 accounting for feedbacks, temperature is more sensitive to the forcing applied in G4Foam than
498 G4SSA. However, global mean surface temperature in G4SSA 0.3 K lower than G4Foam
499 because of a larger change in all-sky top of atmosphere net shortwave flux (Fig. 3).
500 Additionally, the latitudinal distribution of temperature reduction is different in G4Foam than in
501 G4SSA. G4SSA is most effective in cooling the NH continents, while G4Foam most effectively
502 cools the surface south of around 30°N (Fig. 4).

503 Precipitation over land globally, in the tropics, during JJA globally, and during JJA in the
504 tropics is statistically significantly increased in G4Foam relative to both G4SSA and RCP6.0
505 (Fig. 7). The increase in precipitation in G4Foam relative to RCP6.0 is very likely undesirable in
506 areas that already receive a lot of rainfall. The combination of cooling and increased

507 precipitation over land in the tropics results in a statistically significant increase in precipitation
508 minus evaporation on an annual mean basis over Central America, the Northern Amazon, the
509 Sahel, the Indian Subcontinent, the Maritime Continent and Southeast Asia in G4Foam relative
510 to G4SSA (Fig. 8). All of these areas are very densely populated and heavily cultivated. Water
511 scarcity is a major issue in many of these areas and G4Foam describes a climate model response
512 in which there is global cooling, but higher P-E is modeled for many regions, some of which are
513 in need of greater water supply. However, in order to assess actual changes in water supply, it
514 would be necessary to analyze extreme events, as well as the economic and policy issues that
515 ultimately determine the allocation of water resources in a given region.

516 Finally, both the changes in the spatial pattern and magnitude of changes in temperature
517 and precipitation are far too large to be explained by the forcing alone. Instead, much of the
518 temperature and hydrological response is the result of powerful cloud feedbacks and changes in
519 the tropical meridional overturning circulation induced by the placement of the ocean albedo
520 forcing.

521 **4.2 The hydrological response**

522 The dominant cause of the G4Foam hydrological response is the intensification of the
523 southern Hadley Cell and the northward migration of the ITCZ in response to the asymmetric
524 forcing. However, the precipitation response is not zonally homogeneous, as the regional and
525 local mechanisms are also important to the distribution of precipitation.

526 First, we address the increase in precipitation over Central America. For this, we turn to
527 literature concerning the decline of Mayan civilization in Central America. Summer insolation
528 in the NH began to decrease about 5,000 years ago. The ITCZ migrated southward. This
529 southward shift caused rainfall to decrease in the crucial summer growing season. Long
530 droughts and eventually water shortages contributed to the civilization's decline (Poore et al.,
531 2004). In G4Foam, the ITCZ moves northward and the areas in which Mayan civilization
532 flourished, including Belize, Guatemala and parts of Mexico, once again receive a great deal
533 more precipitation. This response is strong and consistent in each ensemble member (Figs. 6-8).

534 The long mid-to-late 20th century Sahel drought was primarily caused by the ITCZ being
535 pushed southward by preferential cooling of the NH (Folland, 1986). In G4Foam, the reverse is
536 true. SH cooling pushes the ITCZ north, which generally explains the G4Foam precipitation
537 increase in the Sahel.

538 A surprising finding is that portions of the Arabian Peninsula equatorward of 20°S
539 experience precipitation increases of up to 1 mm day⁻¹ during the JJA season. However, this
540 northward migration of boreal summer precipitation is evident in the paleoclimate record.
541 Evidence of such precipitation is found in Fleitmann et al. (2003), who showed changes in $\delta^{18}\text{O}$
542 in cave stalagmites in Oman, which indicate increased rainfall in Oman under the influence of
543 northward movement of the ITCZ over the Indian Ocean in periods of relative warmth in the NH
544 relative to the SH.

545 Changes in precipitation over the Maritime Continent are partially attributable to large-
546 scale convergence and rising air in those regions, as they lie longitudinally between G4Foam
547 forcing zones where subsidence is enhanced. However, the Indian Ocean Dipole (IOD) (Cai et
548 al., 2012; Chowadry et al., 2012) and Subtropical Indian Ocean Dipole (SIOD) phenomena
549 discussed below are more likely the key drivers of the precipitation response over the Maritime
550 continent.

551 In its positive phase, the SIOD features anomalously warm SSTs in the southwestern
552 Indian Ocean, east and southeast of Madagascar, and cold anomalies of SST west of Australia.
553 Stronger winds prevail along the eastern edge of the SH subtropical high over the Indian Ocean,
554 which becomes intensified and shifted slightly to the south during positive SIOD events. This

555 results in more evaporation over the eastern Indian Ocean, which cools SSTs in the Indian Ocean
556 east of Australia (Suzuki et al., 2004). In the SIOD negative phase, the opposite is true. There is
557 cooler water in the southwest Indian Ocean, near Madagascar and warmer waters to the east,
558 near Australia (Behera et al., 2001; Reason, 2001).

559 The negative phase of the SIOD features more precipitation in western Australia and the
560 Maritime Continent. This negative SIOD phase is consistent with the SST pattern in the Indian
561 Ocean forced by G4Foam. Therefore, the negative SIOD like mean state in G4Foam appears to
562 play a role in the enhanced rainfall in Northwestern Australia and the Maritime Continent.

563 Based on both local and global changes in circulation, we expected a very large increase
564 in the strength of the Indian Monsoon. In addition to the planetary scale changes associated with
565 the ITCZ and the Hadley cell, the position of the semi-permanent high in the subtropical
566 Southern Indian Ocean also plays a large role in modulating the Indian summer monsoon.
567 Negative SIOD events during boreal winter are often followed by strong Indian summer
568 monsoons. During a negative SIOD event, the subtropical high in the Indian Ocean shifts
569 northeastward as the season shifts from December, January, and February to JJA. This causes a
570 strengthening of the monsoon circulation, intensifying the Hadley Cell locally during the JJA
571 monsoon.

572 A negative IOD is associated with a weakened Asian monsoon and an increase in
573 precipitation over Australia and the Maritime Continent. In G4Foam, advection of cold water in
574 the Somali current into the equatorial western Indian Ocean creates a negative IOD-like response
575 that partially counters the combination of the global scale Hadley cell response and the forced
576 SIOD, dampening the overall increase in the Indian monsoon. This warm west, cold east mean
577 state in the equatorial Indian Ocean resembles a negative IOD mean state and it helps to explain
578 the enhanced precipitation response in the Maritime Continent and the lower than expected
579 increase in precipitation over the Indian subcontinent. The Asian monsoon and precipitation
580 over the Maritime Continent are also governed in part by ENSO. However, no changes in ENSO
581 were evident in G4Foam relative to G4SSA or RCP6.0. There is also no evident response of
582 ENSO amplitude or frequency to any of several different regimes of stratospheric
583 geoengineering (Gabriel and Robock, 2015).

584 **4.3 Caveats**

585 The technology does not presently exist to actually deploy a stable, highly reflective layer
586 of microbubbles on the actual ocean surface. While a stable, highly reflective, nondispersive
587 foam has been developed in a saltwater solution, appropriate for climate engineering, this foam
588 has not been tested outside the laboratory, much less on the surface of a large area of rarely
589 quiescent ocean. The foam has not been immersed in a medium in which bacteria are present,
590 and the interaction between the bacteria and the protein surfactant could damage the layer of
591 microbubbles. Also, even though the diameter of these microbubbles is on the order of 10^{-6} m,
592 the demand for surfactant would likely overwhelm our current production capacity of whatever
593 surfactant is chosen. The research on the engineering required to perform stratospheric
594 geoengineering by sulfate injection is much further along than research of microbubble
595 deployment, which is still in its earliest stages.

596 However, since development of microbubble technology is underway, it is worthwhile to
597 determine how such a technology could be applied in a manner that would address serious
598 climate issues. The progress being made in research associated with stratospheric
599 geoengineering actually enhances the relevance of researching the climate impact of this
600 particular ocean surface geoengineering approach as G4Foam was designed with an eye toward
601 concurrent deployment with stratospheric geoengineering in the event the stratospheric

602 geoengineering were to cause the precipitation deficits that many model studies have shown that
603 it might.

604 More fundamentally, the propriety of any attempt to impose a the G4Foam forcing in an
605 attempt to achieve the modeled G4Foam climate is premised on a value judgment that it is
606 desirable to develop a technology that could redistribute essential resources between nations in
607 an attempt to achieve a net benefit to humanity as a collective when it unknowingly creates a
608 local scarcity of these essential resources. To some extent, making this value judgment is
609 germane and is a prerequisite to the discussion of any form of geoengineering. Even though
610 G4Foam would be successful in increasing P-E in more heavily populated areas, P-E will almost
611 certainly be reduced in remote regions, such as South Pacific islands. Is it ethical to pick
612 winners and losers when the selection process is aimed at increasing the number of winners and
613 decreasing the number of losers? Hypothetically, if G4Foam worked as described in this paper,
614 from a purely consequentialist perspective, and with the sole objective being increased utility for
615 the human collective, G4Foam could be considered beneficial.

616 Finally, this paper is concerned with the climate response to surface albedo changes. We
617 do not examine how placing an actual layer of microbubbles in the ocean would change ocean
618 circulation or impact chemistry and biology in the ocean. Evaluating the changes in the ocean,
619 especially changes in its circulation that are caused by the surface albedo modification, is one of
620 the next issues to explore. The ocean regions we propose to brighten have low biological
621 productivity and weak currents, but the possibility of remote impacts, due to changes in
622 circulation having negative impacts on important ocean regions, is worth considering.

623 **4.4 Future research**

624 Whether or not a concurrent deployment of stratospheric geoengineering and ocean
625 albedo modification could cool the entire planet while maintaining or enhancing the hydrological
626 cycle, particularly in the tropics, is the next natural step in this research. Such research is
627 motivated by the need to determine whether some combination of geoengineering techniques can
628 be used to offset regional climate disparities that using one method of geoengineering alone
629 could induce.

630
631

632 **Acknowledgments.** We thank two anonymous referees for their valuable comments, which
633 improved this manuscript. This work is supported by U.S. National Science Foundation (NSF)
634 grants AGS-1157525, GEO-1240507, and AGS-1617844. Computer simulations were
635 conducted on the National Center for Atmospheric Research (NCAR) Yellowstone
636 supercomputer. NCAR is funded by NSF. The CESM project is supported by NSF and the
637 Office of Science (BER) of the U.S. Department of Energy. The Pacific Northwest National
638 Laboratory is operated for the U.S. Department of Energy by Battelle Memorial Institute under
639 contract DE-AC05-76RL01830.

640

References

- 641
642
- 643 Aswathy, V. N., Boucher, O., Quaas, M., Niemeier, U., Muri, H., Mülmenstädt, J., and Quaas, J.:
644 Climate extremes in multi-model simulations of stratospheric aerosol and marine cloud
645 brightening climate engineering, *Atmos. Chem. Phys.*, 15, 9593-9610, doi:10.5194/acp-15-
646 9593-2015, 2015.
- 647
648 Aziz, A., Hailes, H.C., Ward, J.M. and Evans, J.R.G.: Long-term stabilization reflective foams in
649 seawater. *Royal Society of Chemistry*. 95, 53028–53036. 2014.
- 650
651 Behera, S. K. and Yamagata, T.: Subtropical SST dipole events in the southern Indian Ocean,
652 *Geophysical Research Letters* 28: 327–330, 2001
- 653
654 Bonan, G. B., Lawrence, P. J., Oleson, K. W., Levis, S., Jung, M., Reichstein, M., Lawrence, D.
655 M., and Swenson, S. C.: Improving canopy processes in the Community Land Model version
656 4 (CLM4) using global flux fields empirically inferred from FLUXNET data, *J. Geophys.*
657 *Res.*, 116, G02014, doi:10.1029/2010JG001593, 2011.
- 658
659 Broccoli, A. J., Dahl, K. A. and Stouffer, R.J.: The response of the ITCZ to Northern
660 Hemisphere cooling. *Geophys. Res. Lett.*, 33, L01702, doi:10.1029/2005GL024546, 2006.
- 661
662 Cai W., Van Rensch P., Cowan T. and Hendon H.H.: Teleconnection pathways for ENSO and
663 the IOD and the mechanism for impacts on Australian rainfall, *J. Climate*, 24:3910–3923,
664 doi:10.1175/2011JCLI4129.1, 2011.
- 665
666 Chao, W.C. and Chen, B.: The origin of the monsoons, *J. Atmos. Sci.*, 58, 3497–3507. 2001.
- 667
668 Chiang, J. C. H. and Bitz, C. M. Influence of high latitude ice cover on the marine Intertropical
669 Convergence Zone. *Climate Dynamics* 25, 477–496, 2005.
- 670
671 Chowdary J.S., Xie, S-P, Tokinaga, H., Okumura, Y.M., Kubota H., Johnson N. and Zheng X-
672 T: Interdecadal variations in ENSO teleconnection to the Indo–western Pacific for 1870–
673 2007, *J. Climate*, 25:1722–1744. doi:10.1175/JCLI-D-11-00070.1, 2012.
- 674
675 Crutzen, P.: Albedo enhancement by stratospheric sulfur injections: A contribution to solve a
676 policy dilemma?, *Climatic Change*, 77, 211–219, 2006.
- 677
678 Cvijanovic, I., Caldeira, K., and MacMartin, D.G.: Impacts of ocean albedo alteration on Arctic
679 sea ice restoration and Northern Hemisphere climate, *Environmental Research Letters*, 10,
680 044020, doi:10.1088/1748-9326/10/4/044020, 2015.
- 681
682 DeSzoek, S.P., Verlinden, K.L., Yuter, S.E. and Mechem, D.B.: The Time Scales of Variability
683 of Marine Low Clouds, *J. Climate.*, published online, <http://dx.doi.org/10.1175/JCLI-D-15-0460.1>, 2016.
- 684
685

686 Dykema J.A., Keith D.W., Anderson J.G., Weisenstein, D.: Stratospheric controlled perturbation
687 experiment: a small-scale experiment to improve understanding of the risks of solar
688 geoengineering, *Phil. Trans. R. Soc. A* 372, 20140059, doi:10.1098/rsta.2014.0059, 2014.
689

690 Emori, S. and Brown, S.J.: Dynamic and thermodynamic changes in mean and extreme
691 precipitation under changed climate, *Geophysical Research Letters*, 321,17,
692 doi:10.1029/2005GL023272, 2005.
693

694 Fleitmann, D., Burns, S.J., Mudelsee, M., Neff, U., Kramers, J., Mangini, A., Matter, A., 2003a.
695 Holocene forcing of the Indian monsoon recorded in a stalagmite from Southern Oman,
696 *Science*, 300, 1737–1739.
697

698 Folland, C. K., Parker, D. E and Palmer, T. N.: Sahel rainfall and worldwide sea temperatures
699 1901–85, *Nature*, 320, 602–607, 1986.
700

701 Frierson, D. M. W. and Hwang, Y-T. Extratropical influence on ITCZ shifts in slab ocean
702 simulation of global warming, *J. Clim.*, 25, 720–733, 2012.
703

704 Gabriel, C. J. and Robock, A.: Stratospheric geoengineering impacts on El Niño/Southern
705 Oscillation, *Atmos. Chem. Phys.*, 15, 11949-11966, doi:10.5194/acp-15-11949-2015, 2015.
706

707 George, R. C. and Wood, R.: Subseasonal variability of low cloud radiative properties over the
708 southeast Pacific Ocean, *Atmos. Chem. Phys.*, 10, 4047-4063, doi:10.5194/acp-10-4047-
709 2010, 2010.
710

711 Haywood, J. M., Jones, A., Bellouin, N. and Stephenson, D.: Asymmetric forcing from
712 stratospheric aerosols impacts Sahelian rainfall, *Nat. Clim. Change*, 3(7), 660–665,
713 doi:10.1038/nclimate1857, 2013.
714

715 Held, I. M. and Soden, B. J.: Robust responses of the hydrological cycle to global warming, *J.*
716 *Climate*, 19, 5686–5699, 2006.
717

718 Hurley, J. V. and Boos, W. R.: Interannual variability of monsoon precipitation and local
719 subcloud equivalent potential temperature. *J. Climate*, 26, 9507–9527, 2013.
720

721 Hwang, Y.-T., Frierson, D. M. W. and Kang, S. M.: Anthropogenic sulfate aerosol and the
722 southward shift of tropical precipitation in the late 20th century, *Geophys. Res. Lett.*, 40,
723 doi:10.1002/grl.50502, 2013.
724

725 IPCC: Summary for Policymakers, in: *Climate Change 2013: The Physical Science Basis.*
726 *Contribution of Working Group I to the Fifth Assessment Report of the Intergovernmental*
727 *Panel on Climate Change*, edited by: Stocker, T. F., Qin, D., Plattner, G.-K., Tignor, M.,
728 Allen, S. K., Boschung, J., Nauels, A., Xia, Y., Bex, V., and Midgley, P. M., Cambridge
729 University Press, Cambridge, UK and New York, NY, USA, 2013.
730

731 Irvine, P. J., Ridgwell, A. and Lunt, D. J.: Climatic effects of surface albedo geoengineering, *J.*
732 *Geophys. Res.*, 116, D24112, doi:10.1029/2011JD016281, 2011.
733

734 Kang, S. M., Held, I. M., Frierson, D. M. W and Zhao, M.: The response of the ITCZ to
735 extratropical thermal forcing: Idealized slab-ocean experiments with a GCM, *J.*
736 *Climate*, 21, 3521–3532, 2008.
737

738 Keith, D. W., Duren, R. and MacMartin, D.G.: Field experiments on solar geoengineering: report
739 of a workshop exploring a representative research portfolio. *Philosophical Transactions of*
740 *the Royal Society A.*, 372-20140175, 2014.
741

742 Kravitz, B., Robock, A., Boucher, O., Schmidt, H., Taylor, K., Stenchikov, G. and Schulz, M.:
743 The geoengineering model intercomparison project (GeoMIP), *Atm. Sci. Lett.*, 12, 162-167,
744 doi: 10.1002/asl.316. 201, 2011.
745

746 Kravitz, B., Robock, A., Tilmes, S., Boucher, O., English, J. M., Irvine, P. J., Jones, A.,
747 Lawrence, M. G., MacCracken, M., Muri, H., Moore, J. C., Niemeier, U., Phipps, S. J.,
748 Sillmann, J., Storelvmo, T., Wang, H., and Watanabe, S.: The Geoengineering Model
749 Intercomparison Project Phase 6 (GeoMIP6): simulation design and preliminary results,
750 *Geosci. Model Dev. Discuss.*, 8, 4697–4736, doi:10.5194/gmdd-8-4697-2015, 2015.
751

752 Jones A., Haywood, J. and Boucher, O.: Climate impacts of geoengineering marine
753 stratocumulus clouds, *J. Geophys. Res.*, 114, D10106, doi:10.1029/2008JD011450, 2009.
754

755 Kay J. E., Wall C., Yettella V., Medeiros B., Hannay C., Caldwell P. and Bitz C.: Global
756 climate impacts of fixing the Southern Ocean shortwave radiation bias in the community
757 earth system model (CESM), *J. Climate*, doi:10.1175/JCLI-D-15-0358, 2016.
758

759 Kharin, V. V., Zwiers, F. W., Zhang, X., and Hegerl, G. C.: Changes in temperature and
760 precipitation extremes in the IPCC ensemble of Global Coupled Model Simulations, *J.*
761 *Climate*, 20, 1419– 1444, doi:10.1175/JCLI4066.1, 2007.
762

763 Lamarque, J-F., Emmons, L. K., Hess, P. G., Kinnison, D. E., Tilmes, S., Vitt, F., Heald, C. L.,
764 Holland, E. A., Lauritzen, P. H., Neu, J., Orlando, J. J., Rasch, P. J., and Tyndall, G. K.:
765 CAM-chem: description and evaluation of interactive atmospheric chemistry in the
766 Community Earth System Model, *Geosci. Model Dev.*, 5, 369–411, doi:10.5194/gmd-5-369-
767 2012, 2012.
768

769 Latham, J., Bower, K., Choulaton, T., Coe, H., Connoly, P., Cooper, G., Craft, T., Foster, J.,
770 Gadian, A., Galbraith, L., Iacovides, H., Johnston, D., Launder, B., Leslie, B., Meyer, J.,
771 Neukermans, A., Ormond, B., Parkes, B., Rasch, P., Rush, J., Salter, S., Stevenson, T.,
772 Wang, H., Wang, Q., and Wood, R.: Marine cloud brightening, *Phil. Trans. R. Soc. A*, 370,
773 4217–4262, doi:10.1098/rsta.2012.0086, 2012.
774

775 Manabe, S. and Stouffer, R. J.: Sensitivity of a global climate model to an increase of CO₂
776 concentration in the atmosphere. *J. Geophys. Res.* 85, 5529–5554, 1980.
777

778 Mechoso, C., Wood, R., Weller, R., Bretherton, C. S., Clarke, A., Coe, H., Fairall, C., Farrar, J.
779 T., Feingold, G. and Garreaud, R.: Ocean-cloud-atmosphere-land interactions in the
780 southeastern Pacific: The VOCALS Program, *Bull. Amer. Meteor. Soc.*, 95, 357-375, 2014.
781

782 Meehl, G. A., Arblaster, J. M., Caron, J. M., Annamalai, H., Jochum, M., Chakraborty, A., and
783 Murtugudde, R.: Monsoon regimes and processes in CCSM4. Part I: The Asian-Australian
784 Monsoon, *J. Climate*, 25, 2583–2608, 2012.

785
786 Meinshausen, M., Smith, S. J., Calvin, K., Daniel, J. S., Kainuma, M. L. T., Lamarque, J.-F.,
787 Matsumoto, K., Montzka, S. A., Raper, S. C. B., Riahi, K., Thomason, A., Velders, G. J. M.,
788 and van Vuuren, D. P. P.: The RCP greenhouse gas concentrations and their extension from
789 1765 to 2300, *Climatic Change*, 109, 213– 241, doi:10.1007/s10584-011-0156-z, 2011.

790
791 Neale, R., Richter, J., Park, S., Lauritzen, P., Vavrus, S., Rasch, P. and Zhang, M.: The mean
792 climate of the Community Atmosphere Model (CAM4) in forced SST and fully coupled
793 experiments, *J. Climate*, 26, 5150–5168, 2013.

794
795 Neely III, R. R., Conley, A. J., Vitt, F., and Lamarque, J.-F.: A consistent prescription of
796 stratospheric aerosol for both radiation and chemistry in the Community Earth System Model
797 (CESM1), *Geosci. Model Dev.*, 9, 2459-2470, doi:10.5194/gmd-9-2459, 2016.

798
799 Poore, R. Z., Quinn, T.M. and Verardo, S.: Century-scale movement of the Atlantic Intertropical
800 Convergence Zone linked to solar variability, *Geophys. Res. Lett.*, 31, L12214, doi:
801 10.1029/2004GL019940, 2004.

802
803 Rasch P. J., Latham, J. and Chen, C.C.: Geoengineering by cloud seeding: influence on sea ice
804 and climate system, *Environmental Research Letters*, 4, 45-112. doi:10.1088/1748-
805 9326/4/4/045112, 2009.

806
807 Reason, C. J. C.: Subtropical Indian Ocean SST dipole events and southern African rainfall,
808 *Geophys. Res. Lett.*, 28, 2225-2228, 10.1029/2000GL012735, 2001.

809
810 Robock, A.: 20 reasons why geoengineering may be a bad idea, *Bull. Atomic Sci.*, 64, 14–18,
811 doi:10.2968/064002006, 2008.

812
813 Robock, A.: Bubble, bubble, toil and trouble. An editorial comment. *Climatic Change*, 105, 383-
814 385, doi:10.1007/s10584-010-0017-1, 2011.

815
816 Robock, A.: Stratospheric aerosol geoengineering, *Issues Env. Sci. Tech.* (special issue
817 “Geoengineering of the Climate System”), 38, 162-185, 2014.

818
819 Robock, A.: Albedo enhancement by stratospheric sulfur injection: More research needed.
820 *Earth’s Future*, doi:10.1002/2016EF000407, 2016.

821
822 Sanderson B.M., O’Neill B., Tebaldi C.: What would it take to achieve the Paris temperature
823 targets? *Geophys Res Lett*, 1, 10., doi:10.1002/2016GL069563, 2016.

824
825 Seitz, R.: Bright water: hydrosols, water conservation and climate change. *Climatic Change*,
826 105, 365–381, 2010.

827

828 Siegenthaler, U., Stocker, T. F., Monnin, E., Luthi, D., Schwander J., Stauffer, B., Raynaud, D.,
829 Barnola, J. M., Fischer, H., Masson, Delmotte, V., and Jouzel, J.: Stable carbon cycle-climate
830 relationship during the late Pleistocene, *Science*, 310, 1313–1317, 2005.
831

832 Suzuki, R., Behera, S.K., Iizuka, S. and Yamagata, T.: The Indian Ocean subtropical dipole
833 simulated using a CGCM, *J. Geo. Res.* 109, doi:10.1029/2003JC001974, 2004.
834

835 Taylor, K. E., Stouffer, R. J., and Meehl, G. A.: An overview of CMIP5 and the experiment
836 design, *B. Am. Meteorol. Soc.*, 93, 485–498, doi:10.1175/BAMS-D-11-00094.1, 2012.
837

838 Tilmes, S., Fasullo, J., Lamarque, J.-F., Marsh, D. R., Mills, M., Alterskjaer, K., Muri, H.,
839 Kristjánsson, J. E., Boucher, O., Schulz, M., Cole, J. N. S., Curry, C. L., Jones, A., Haywood,
840 J., Irvine, P. J., Ji, D., Moore, J. C., Karam, D. B., Kravitz, B., Rasch, P. J., Singh, B., Yoon,
841 J.-H., Niemeier, U., Schmidt, H., Robock, A., Yang, S., and Watanabe, S.: The hydrological
842 impact of geoengineering in the Geoengineering Model Intercomparison Project (GeoMIP),
843 *J. Geophys. Res.-Atmos*, 118, 11036–11058, doi:10.1002/jgrd.50868, 2013.
844

845 Tilmes, S., Mills, M. J., Niemeier, U., Schmidt, H., Robock, A., Kravitz, B., Lamarque, J.-F.,
846 Pitari, G., and English, J. M.: A new Geoengineering Model Intercomparison Project
847 (GeoMIP) experiment designed for climate and chemistry models, *Geosci. Model Dev.*, 8,
848 43-49, doi:10.5194/gmd-8-43-2015, 2015.
849

850 Tilmes, S., Lamarque, J.-F., Emmons, L. K., Kinnison, D. E., Marsh, D., Garcia, R. R., Smith, A.
851 K., Neely, R. R., Conley, A., Vitt, F., Val Martin, M., Tanimoto, H., Simpson, I., Blake, D.
852 R., and Blake, N.: Representation of the Community Earth System Model (CESM1) CAM4-
853 chem within the Chemistry-Climate Model Initiative (CCMI), *Geosci. Model Dev.*, 9, 1853-
854 1890, doi:10.5194/gmd-9-1853-2016, 2016.
855

856 Trenberth, K. E., and Dai, A.: Effects of Mount Pinatubo volcanic eruption on the hydrological
857 cycle as an analog of geoengineering, *Geophys. Res. Lett.*, 34, L15702,
858 doi:10.1029/2007GL030524, 2007.
859

860 Wood, R. and Bretherton, C. S.: Boundary layer depth, entrainment, and decoupling in the cloud-
861 capped subtropical and tropical marine boundary layer, *J. Climate*, 17, 3576–3588, 2004.
862

863 Wood, R. and Bretherton, C. S.: On the relationship between stratiform low cloud cover and
864 lower-tropospheric stability, *J. Climate*, 19, 6425–6432, 2006.
865

866 Xia, L., Robock, A., Tilmes, S., and Neely III, R. R.: Stratospheric sulfate geoengineering could
867 enhance the terrestrial photosynthesis rate, *Atmos. Chem. Phys.*, 16, 1479-1489,
868 doi:10.5194/acp-16-1479-2016, 2016.
869

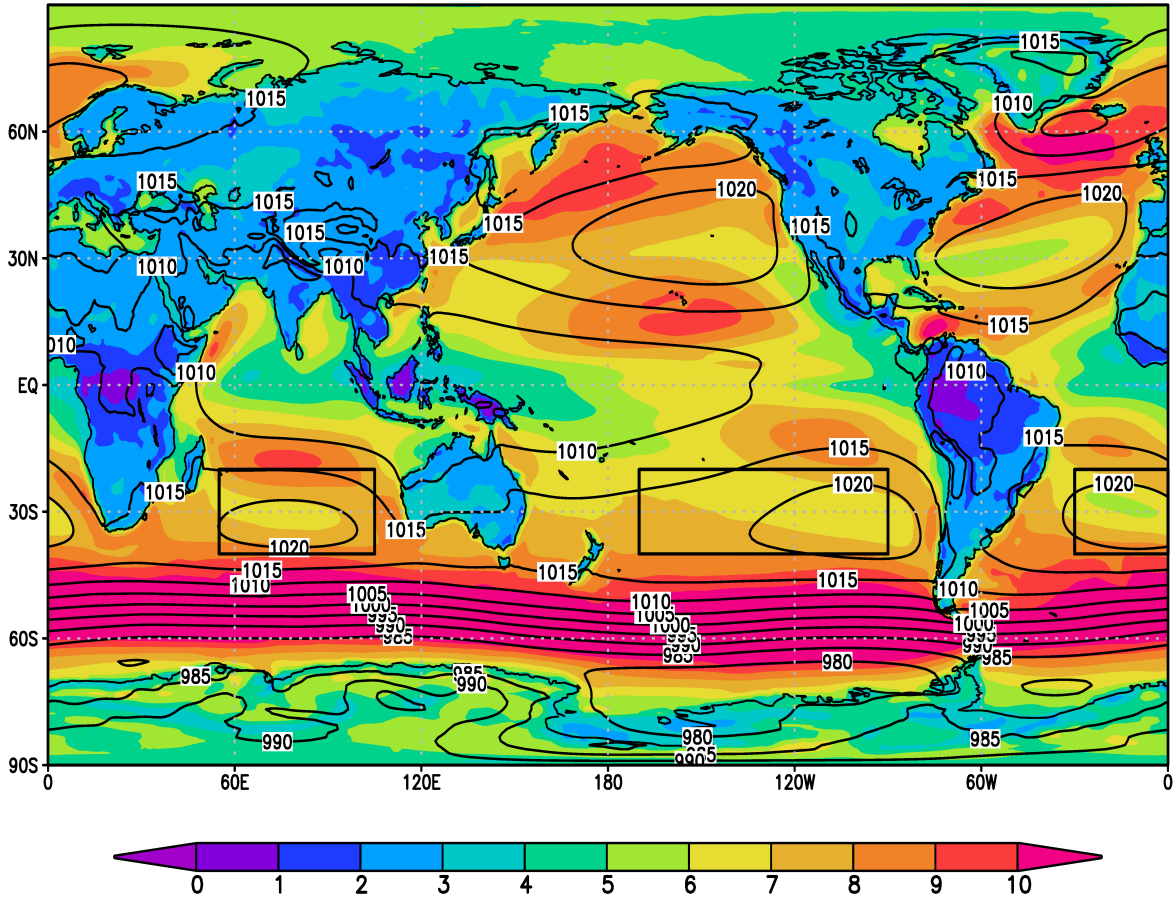
870 Xie, S-P. and Philander, S. G. H., A coupled ocean-atmosphere model of relevance to the ITCZ
871 in the eastern Pacific, *Tellus*, 46A, 340–350, 1994.
872

873 **Table 1.** Changes in temperature and precipitation in G4Foam relative to both G4SSA and
874 RCP6.0, for the entire globe and for the Tropics (20°S-20°N) annually and in Northern
875 Hemisphere summer, for the 40-year period beginning 10 years after the start of climate
876 engineering.
877

| Global, 2030-2069 | G4Foam – G4SSA (% change) | G4Foam – RCP6.0 (% change) |
|--|--------------------------------------|---------------------------------------|
| Precipitation (mm/day) | +0.02 (+0.61) | -0.06 (-1.98) |
| Land precipitation (mm/day) | +0.07 (+3.19) | +0.01 (+0.32) |
| Ocean precipitation (mm/day) | -0.01 (-0.36) | -0.08 (-2.57) |
| Temperature (K) | +0.27 | -0.53 |
| Land temperature (K) | +0.63 | -0.44 |
| Global, 2030-2069, June-July-August | | |
| Precipitation (mm/day) | +0.02 (+0.70) | -0.05 (-1.85) |
| Land precipitation (mm/day) | +0.08 (+3.35) | +0.02 (+0.70) |
| Ocean precipitation (mm/day) | +0.01 (-0.29) | -0.08 (-2.51) |
| Temperature (K) | +0.32 | -0.60 |
| Land temperature (K) | +0.71 | -0.53 |
| Tropical, 2030-2069 | | |
| Precipitation (mm/day) | +0.06 (+1.59) | -0.03 (-1.06) |
| Land precipitation (mm/day) | +0.16 (+3.93) | +0.07 (+1.43) |
| Ocean precipitation (mm/day) | +0.03 (+0.77) | -0.07 (-1.92) |
| Temperature (K) | +0.21 | -0.60 |
| Land temperature (K) | +0.43 | -0.61 |
| Tropical, 2030-2069, June-July-August | | |
| Precipitation (mm/day) | +0.06 (+1.52) | -0.03 (-0.84) |
| Land precipitation (mm/day) | +0.16 (+4.66) | +0.07 (+2.02) |
| Ocean precipitation (mm/day) | +0.03 (+0.67) | -0.06 (-1.61) |
| Temperature (K) | +0.18 | -0.61 |
| Land temperature (K) | +0.37 | -0.70 |

878

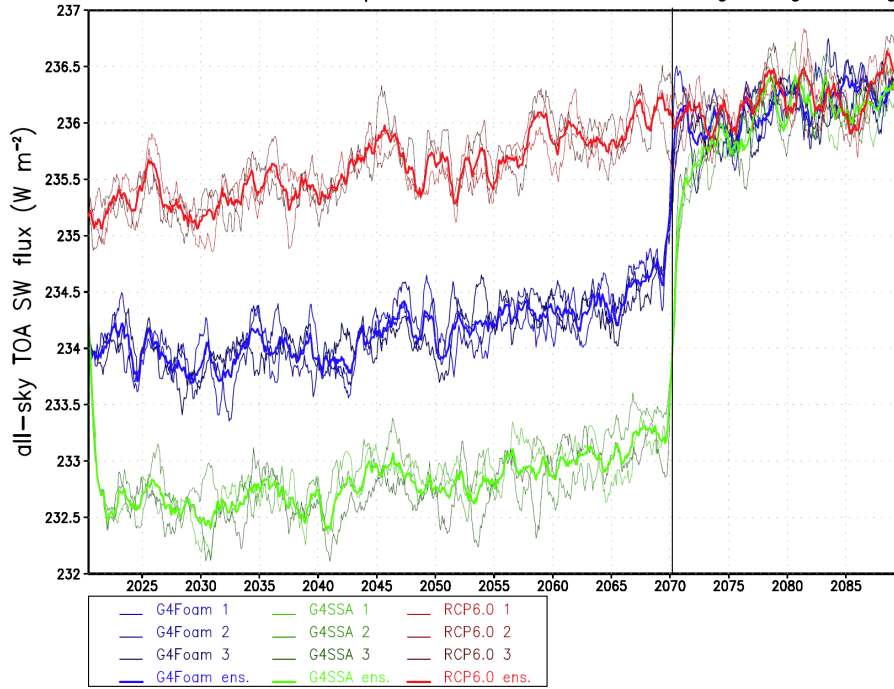
CESM-CAM4-CHEM Control 10m wind (m/s)
 shaded, sea level pressure (hPa) contours
 2005-2019. Boxes bound foamed regions.



879
 880
 881
 882
 883
 884
 885
 886

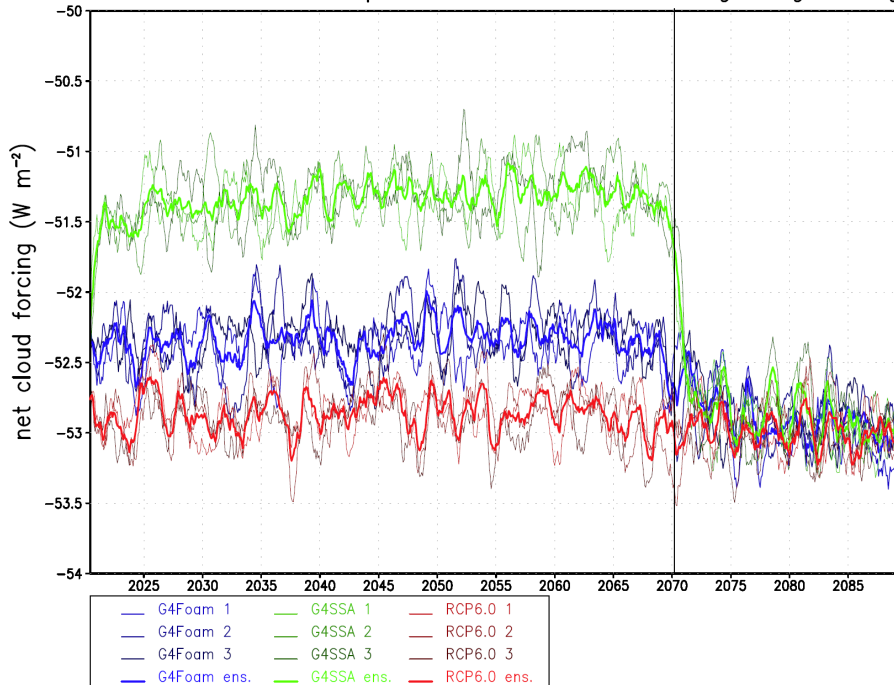
Figure 1. Applied forcing and global mean temperature response. Ocean albedo changed from a daily average of 0.06, which includes a very small daily cycle, to a fixed value of 0.15 with no daily cycle, over “foam regions,” 20°N-20°S, 90°W-170°W (South Pacific), 20°N-20°S, 30°W-0°E (South Atlantic) and 20°N-20°S, 55°E-105°E (South Indian). Each foamed region is outlined in black. Control run sea level pressure (mb) is shown with contours and 10-m winds (m/s) are shaded.

a) 1-year running mean global net all-sky solar flux ($W m^{-2}$), 2020–2089. Line on plot indicates cessation of geoengineering



887
888

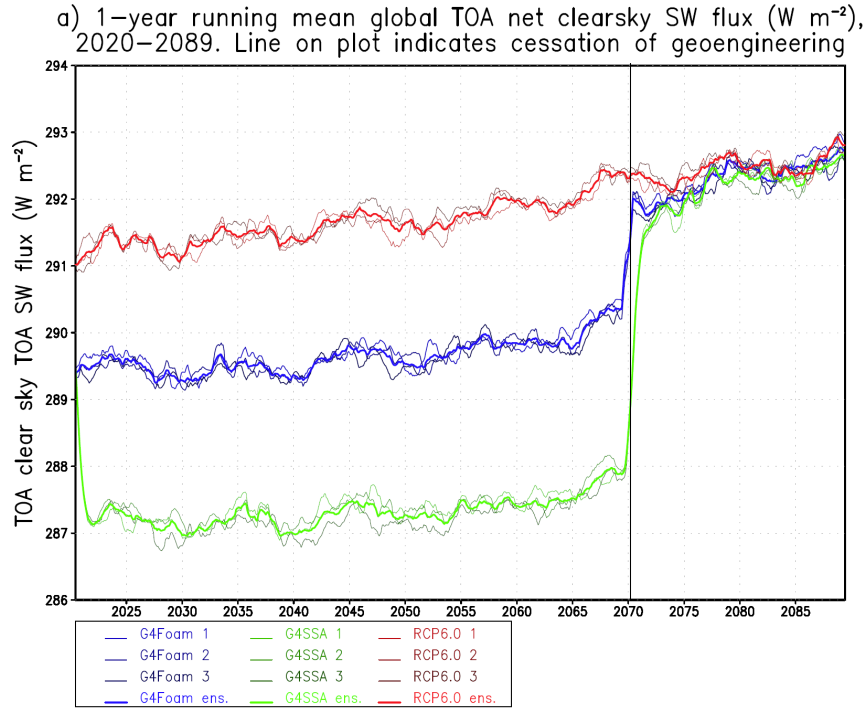
b) 1-year running mean global net cloud forcing ($W m^{-2}$), 2020–2089. Line on plot indicates cessation of geoengineering



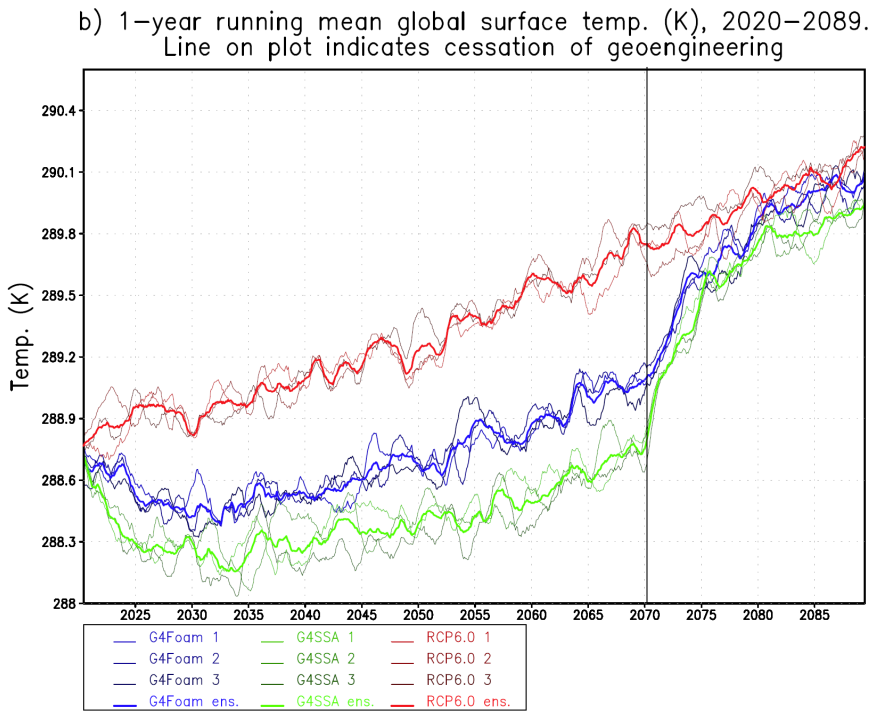
889
890

891 **Figure 2.** a) Net all-sky SW flux at top-of-atmosphere and (b) Time series of global mean net
892 cloud forcing. Each ensemble member and the ensemble mean are shown for each forcing.

893
894

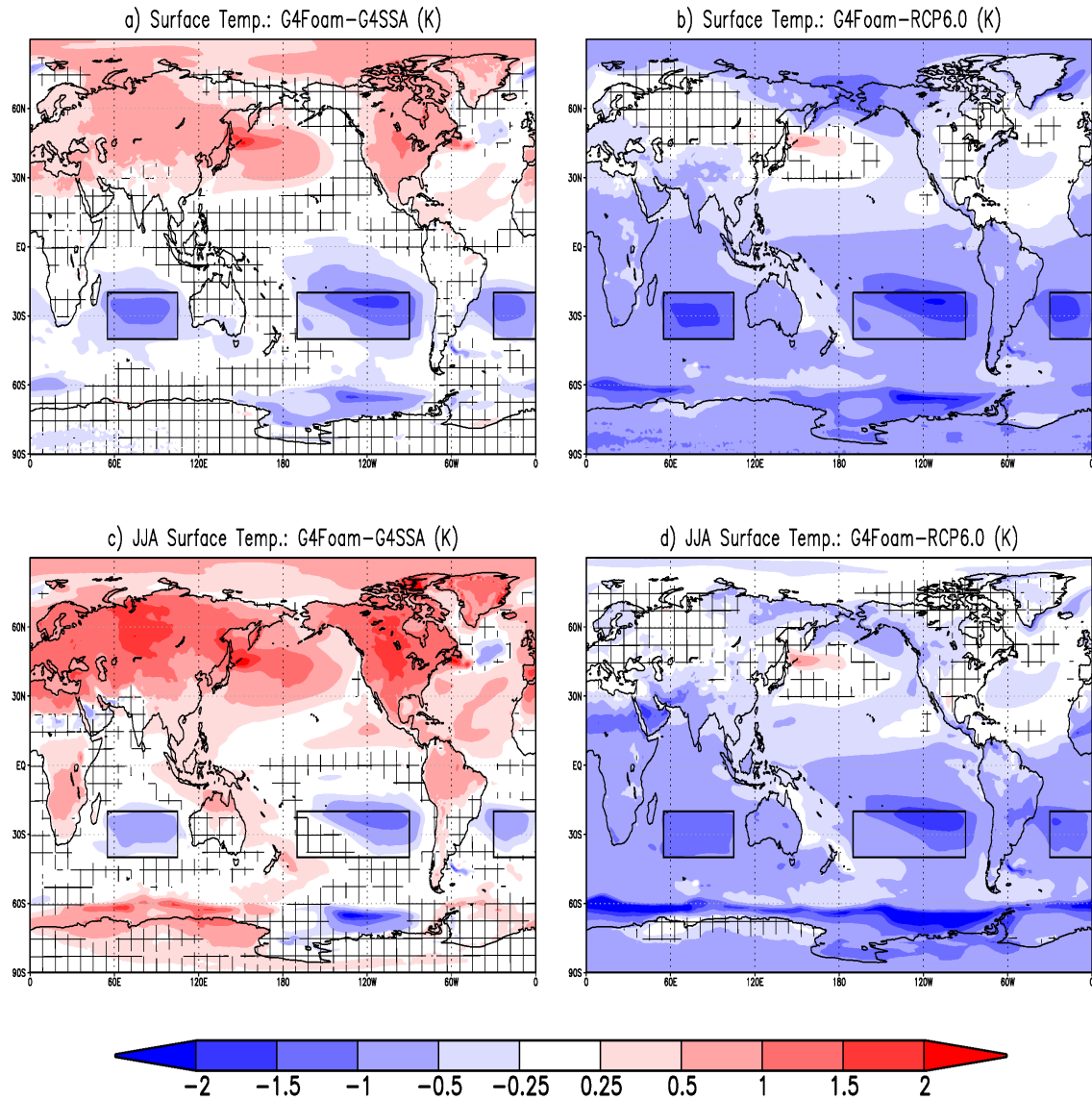


895
896



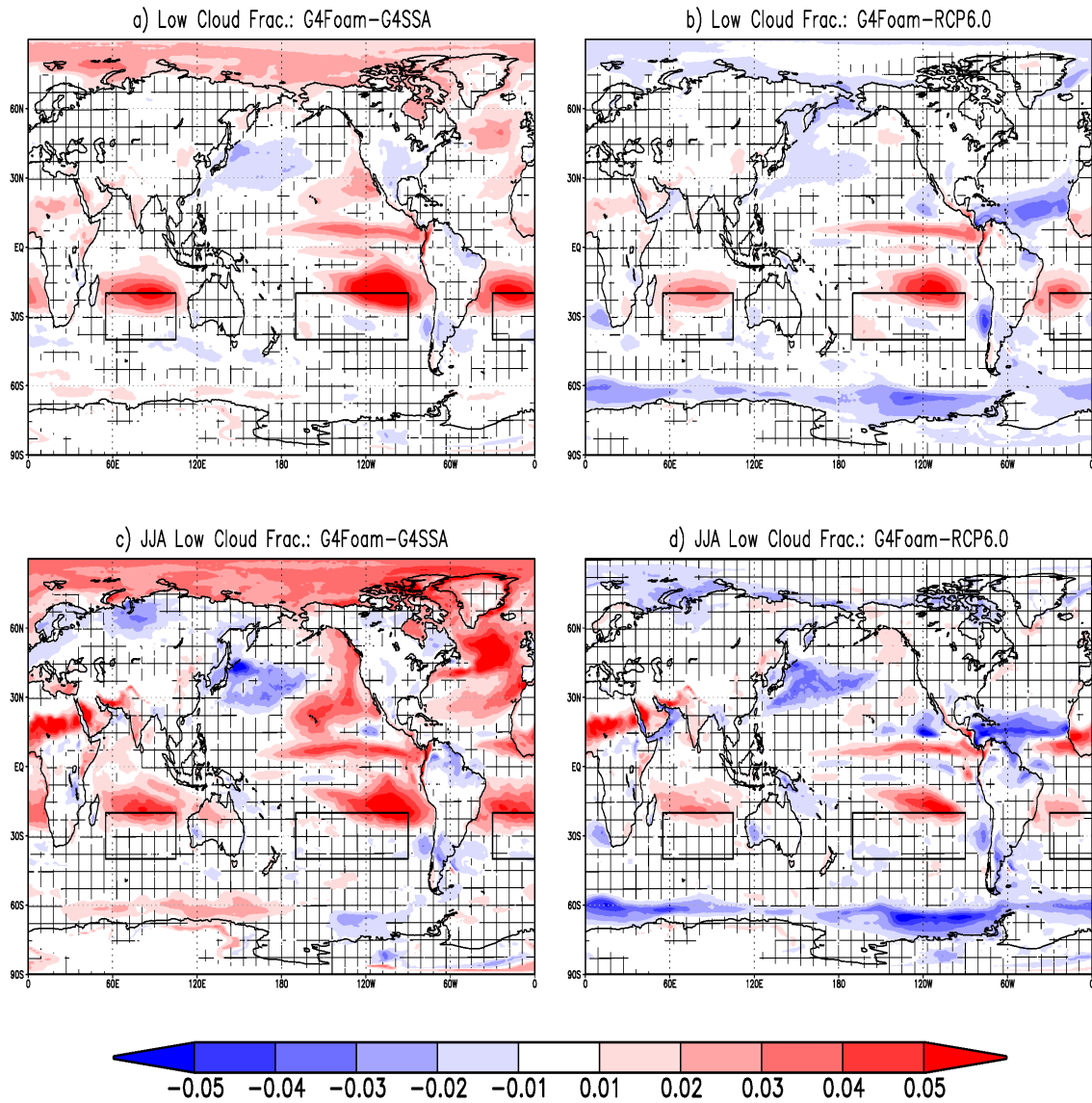
897
898

899 **Figure 3.** (a) Net clear sky SW flux at top of atmosphere, which includes the effects of changes
900 in radiation caused by changes in ocean surface albedo or land albedo (ice and snow), as well as
901 stratospheric aerosols (stratospheric geoengineering) and (b) Time series of global mean
902 temperature. In G4Foam, temperature is more than twice as sensitive to ocean albedo forcing as
903 it is to stratospheric geoengineering, as applied in G4SSA, albeit with very different latitudinal
904 distributions of temperature changes. Each ensemble member and the ensemble mean are shown
905 for each forcing.



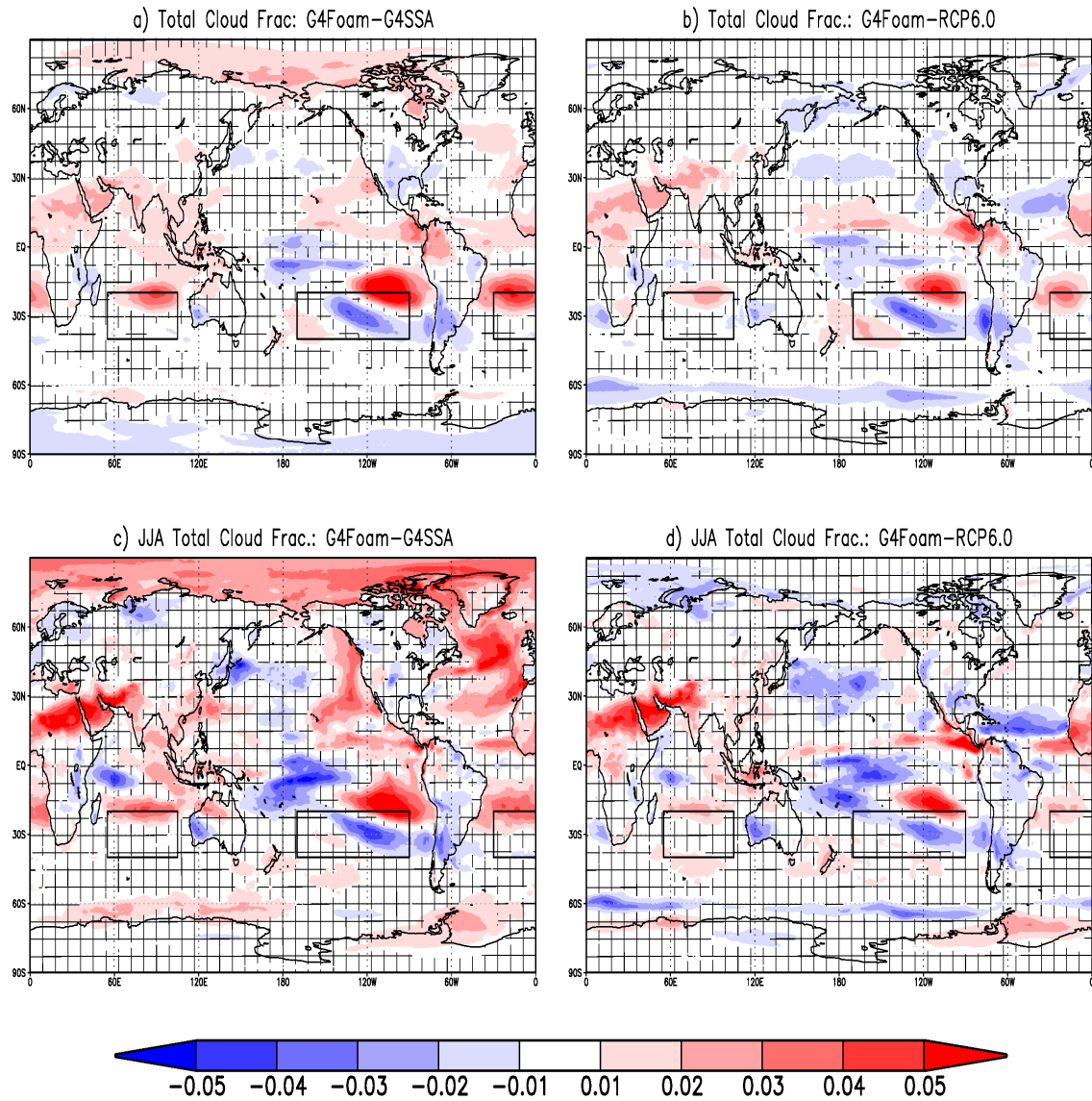
906
 907
 908
 909
 910
 911
 912

Figure 4. 2030-2069 surface temperature differences (K) between G4Foam and (a) G4SSA, (b) RCP6.0, (c) G4SSA during JJA, and (d) RCP6.0 during JJA. Hatched regions are areas with $p > 0.05$ (where changes are not statistically significant based on a paired t -test). Black boxes enclose foamed regions.



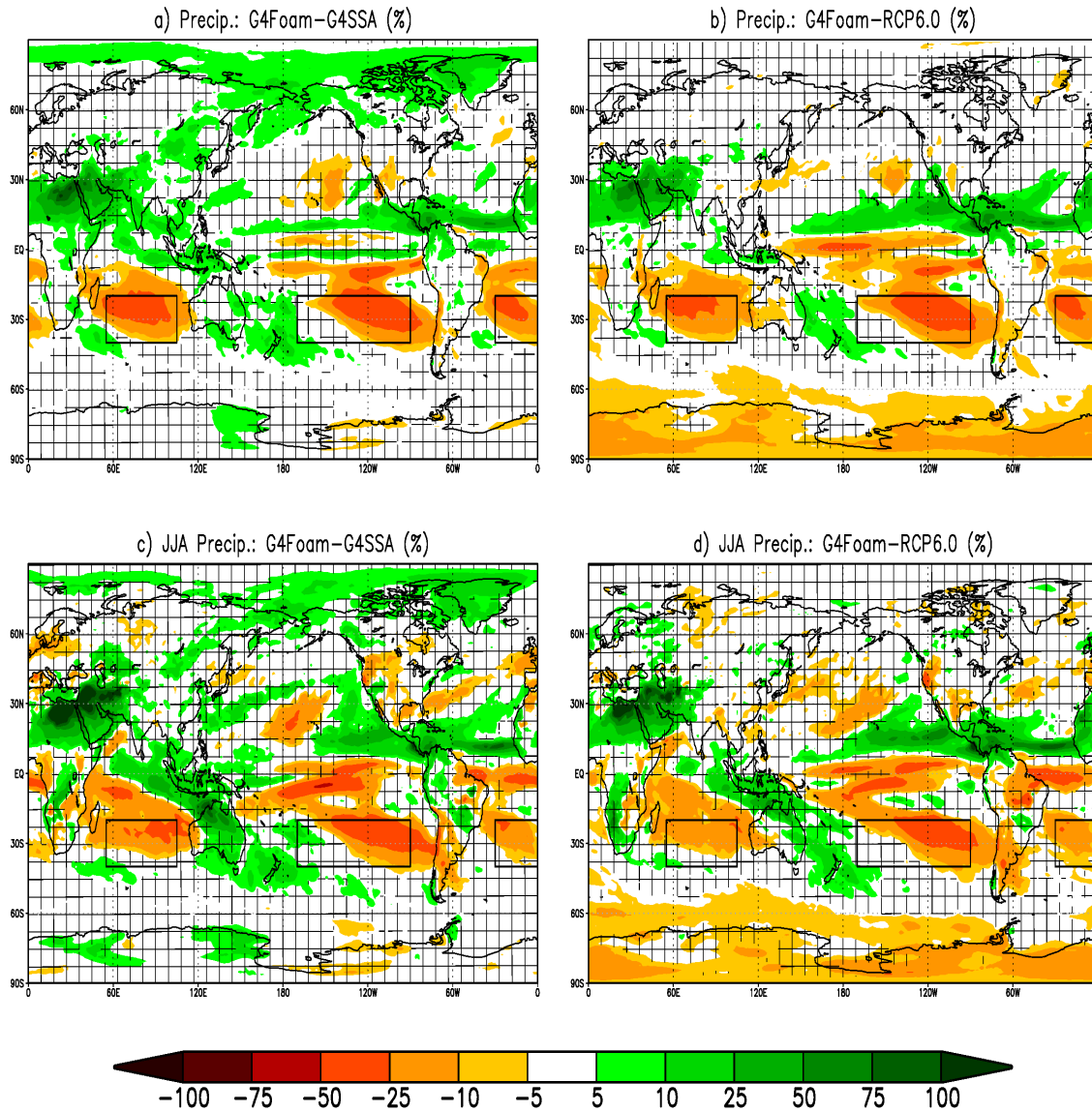
913
 914
 915
 916
 917
 918
 919
 920
 921

Figure 5. 2030-2069 low cloud fraction difference (unitless) between G4Foam and (a) G4SSA, (b) RCP6.0, (c) G4SSA during JJA, and (d) RCP6.0 during JJA. Hatched regions are areas with $p > 0.05$ (where changes are not statistically significant based on a paired t -test). Black boxes enclose foamed regions.



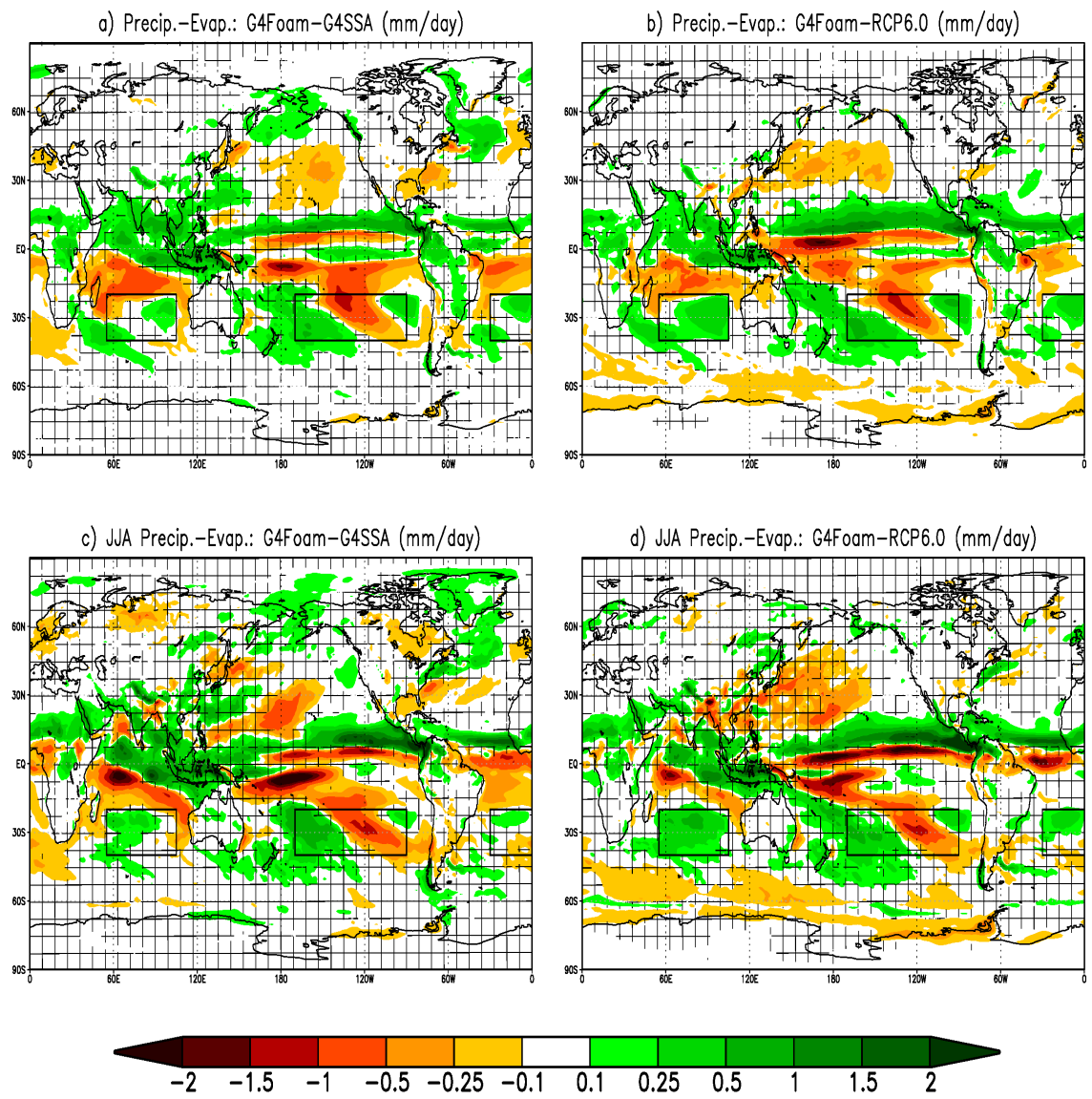
922
 923
 924
 925
 926
 927
 928
 929

Figure 6. 2030-2069 total cloud fraction difference (unitless) between G4Foam and (a) G4SSA, (b) RCP6.0, (c) G4SSA during JJA and (d) RCP6.0 during JJA. Hatched regions are areas with $p > 0.05$ (where changes are not statistically significant based on a paired t -test). Black boxes enclose foamed regions.



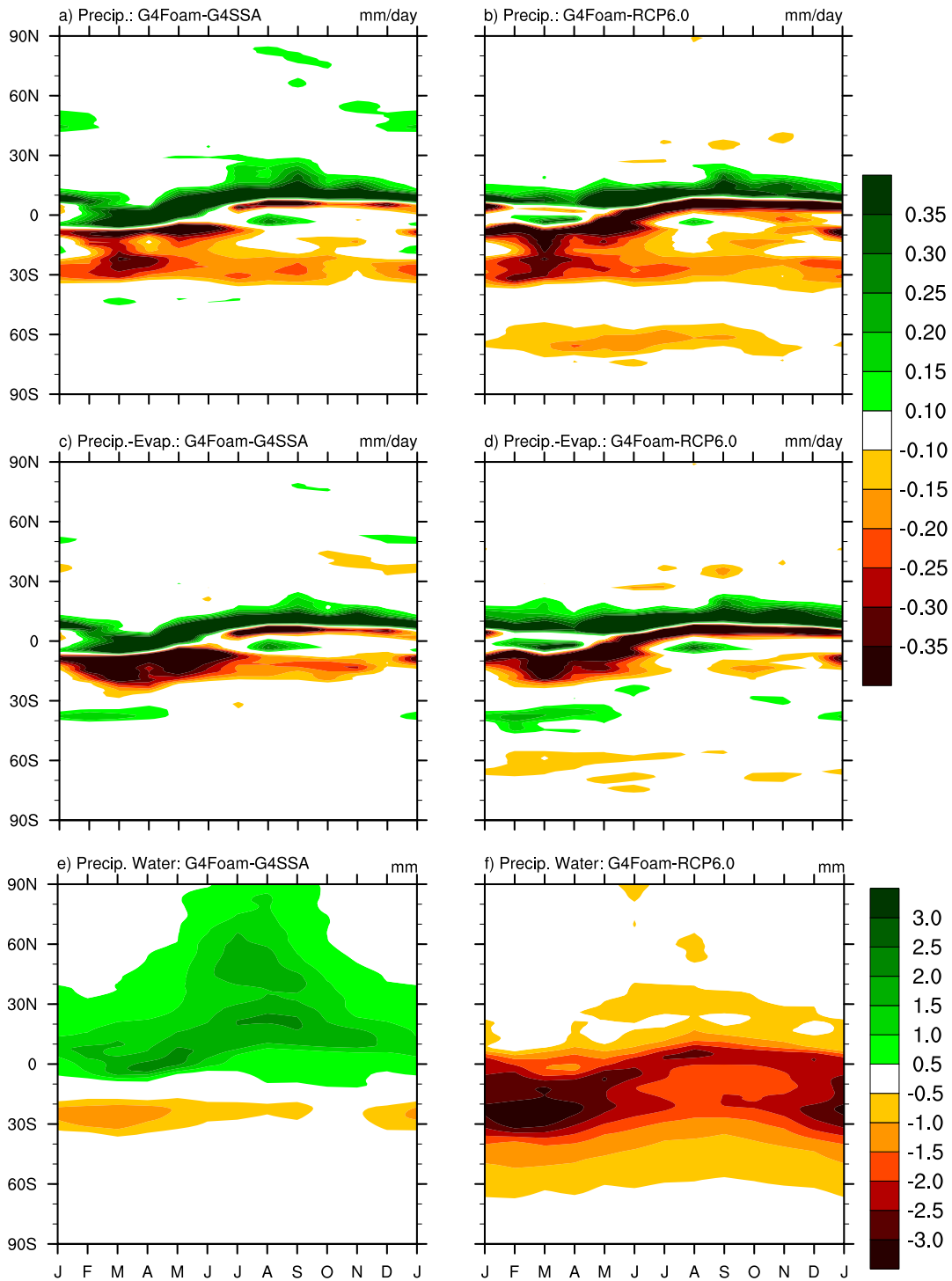
930
 931
 932
 933
 934
 935
 936
 937

Figure 7. 2030-2069 precipitation difference (%) between G4Foam and (a) G4SSA, (b) RCP6.0, (c) G4SSA during JJA and (d) RCP6.0 during JJA. Hatched regions are areas with $p > 0.05$ (where changes are not statistically significant based on a paired t -test). Black boxes enclose foamed regions.

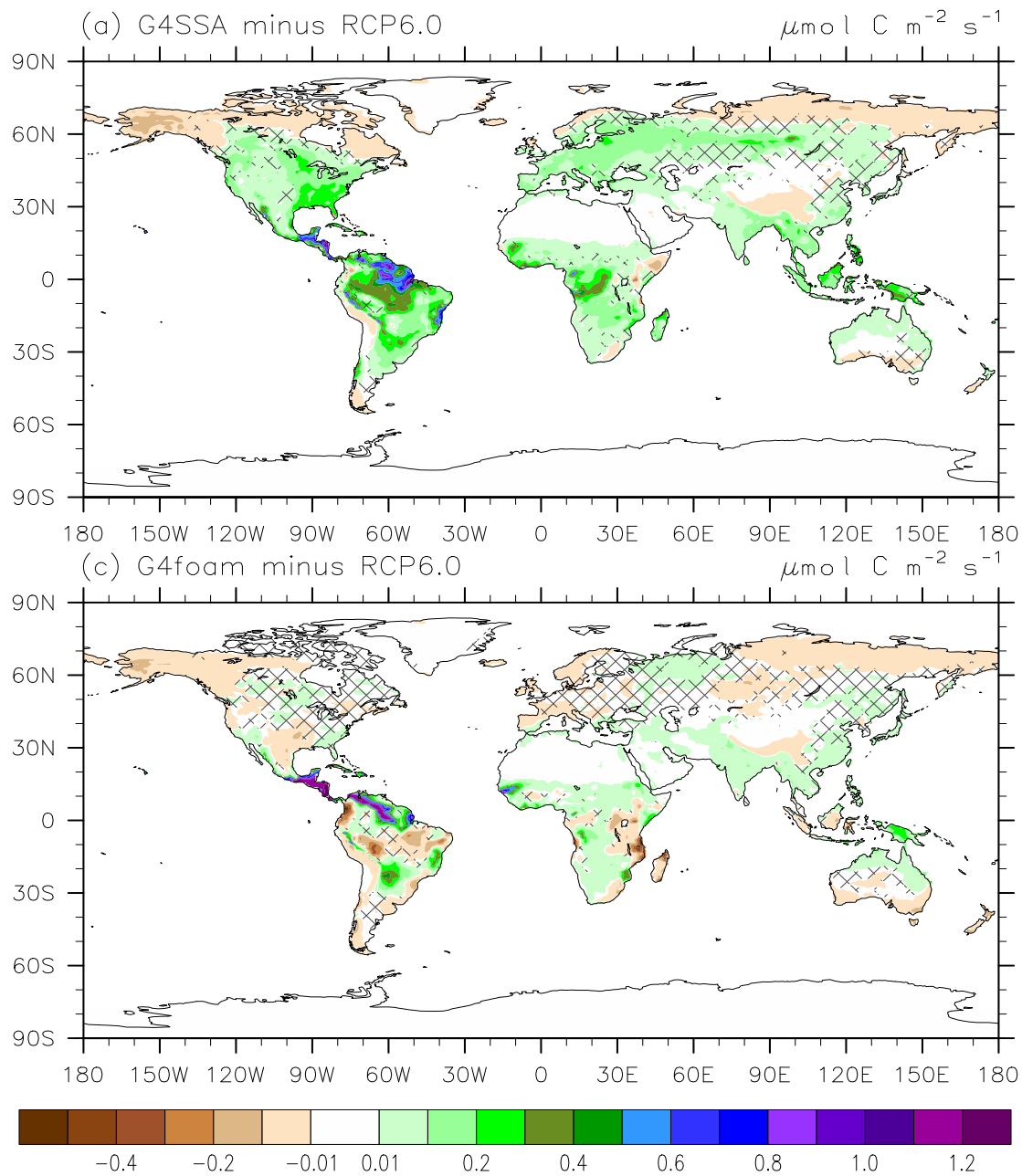


938
 939
 940
 941
 942
 943
 944

Figure 8. 2030-2069 precipitation minus evaporation difference (mm/day) between G4Foam and (a) G4SSA, (b) RCP6.0, (c) G4SSA during JJA and (d) RCP6.0 during JJA. Hatched regions are areas with $p > 0.05$ (where changes are not statistically significant based on a paired t -test). Black boxes enclose foamed regions.



945
 946 **Figure 9.** 2030-2069 monthly mean annual cycle of zonal mean precipitation (mm/day) for (a)
 947 G4Foam minus G4SSA and (b) G4Foam minus RCP6.0, precipitation minus evaporation
 948 (mm/day) for (c) G4Foam minus G4SSA and (d) G4Foam minus RCP6.0, and total precipitable
 949 water (mm) for (e) G4Foam minus G4SSA and (f) G4Foam minus RCP6.0.
 950



951
 952 **Figure 10.** (a) Photosynthesis rate differences between G4SSA and RCP6.0 during years 2030–
 953 2069 (sulfate injection period, excluding the first 10 years) (Fig. 4a from Xia et al., 2016). (b)
 954 Photosynthesis rate anomaly between G4Foam and RCP6.0 during years 2030–2069 of solar
 955 reduction. Hatched regions are areas with $p > 0.05$ (where changes are not statistically
 956 significant based on a paired t test).